4.H_2 adsorption on CuCHA

4.1 Introduction

Metal exchanged zeolites have been suggested as promising candidates for H_2 storage,[1,2] the reversible molecular hydrogen storage being critical for large-scale applications of hydrogen as fuel. The shape of the channels, the high surface area, as well as the interaction between H_2 and the metal cation coordinated to the zeolite framework are determinant factors to control these properties.

From an experimental point of view several efforts have been done to analyse the potentiality of zeolites for H_2 storage. It has been shown that microporous materials, such as zeolites, display appreciable adsorption capabilities.[2] On the other hand, H_2 adsorption in metal exchanged zeolites has been studied from IR experiments.[3,4] In particular, Otero-Areán et al. have studied the H_2 adsorption at low temperatures on Li^+ exchanged ZSM-5. They have observed that the H-H stretching band appears at 4092 cm^{-1} and the adsorption energy is evaluated to be –1.5 kcal/mol.[3] In addition, Spoto et al. have studied the H_2 adsorption on Cu exchanged zeolites.[4] They have observed that, even at room temperatures, the H-H stretching band on H_2-CuZSM-5 appears at 3079 cm^{-1}, which is associated with a really large red shift of 1081 cm^{-1} and a reasonably strong interaction.

From a theoretical point of view the nature of the interaction in several M-H_2^+ systems has been analysed.[5-10] These studies have shown that the inclusion of electron correlation is essential to describe the interaction of H_2 with transition metal cations. Moreover, DFT methods have been shown to be a good chance for studying these systems. In particular, Bowers et al.[6] used DFT on the Cu^+-H_2 system and their obtained results were in excellent agreement with those reported by Bauschlischer et al.[7] using CCSD(T) with very large basis sets. Several factors have been determined to be essential in the metal-H_2 interaction:[6,11] the cost of sd and dp hybridisation, the metal-ligand repulsion, the extent of electron donation and back-donation and finally the charge-induced dipole and charge-quadrupole electrostatic interactions. Thus, the M-H_2^+ binding energy is highly sensitive to the electronic structure of the metal cation.

In zeolites, metal cations act as charge balancing ions of the negatively charged framework by coordinating to the lattice oxygen atoms so that, their electronic properties can experience changes that ultimately could affect their interactions with adsorbed molecules such as H_2.[12] These changes vary depending on the coordination environment

of the metal. Therefore, the metal ability to bind H_2 can strongly depend on the metal cation site. In order to analyse the potentiality of a particular zeolite as a H_2 storage material it is important to know the coordination, accessibility and binding properties of the metal cation at the different positions where it can be located. For that, periodic calculations need to be performed.

To our knowledge, till now no study referring to the H_2 adsorption on metal exchanged zeolites from a theoretical point of view has been reported. Only a few articles discussing the possible location of Cu^+ cations in several zeolites can be considered as related literature.[13-17] It should be mentioned that most of the theoretical studies performed up to now on metal exchanged zeolites have used the cluster approach. Only Sauer et al.[13,14] and Limtrakul et al.[15] have introduced periodic conditions to Cu exchanged zeolites using embedded cluster approaches with different QM/MM schemes. Thus, the present work reports for the first time a fully periodic ab initio simulation on transition metal exchanged zeolite.

Periodic calculations have been performed during two stays in the University of Torino under the supervision of Prof. Piero Ugliengo.

4.2 Goal

The aim of the present chapter is to analyse the possible coordination sites of Cu^+ cations on Chabazite and the subsequent adsorption of one H_2 molecule per copper cation using a fully periodic ab initio simulation. We have chosen Chabazite because it has a small unit cell, which allows performing fully ab initio periodic calculations. Cu^+ has been considered as a metal compensating ion, because gas phase calculations on Cu^+-H_2 have shown that the binding energy is significantly larger (15.4 kcal/mol)[6] than for other cations such as Li^+ (1.45 kcal/mol)[6] or Na^+ (2.45 kcal/mol).[6] Moreover, the analysis of the metal-H_2 interaction is accomplished by modellizing the zeolite with a cluster. The comparison between the cluster and periodic results allows the evaluation of the zeolite long-range effects

4.3 Computational details

Periodic ab initio simulations using localized basis sets based on Gaussian expansion of crystalline orbitals are performed on Chabazite with a Si/Al ratio of 11. That is, one of the 12 silicons of the unit cell[18] has been substituted by aluminium. One Cu^+ is added per unit cell to neutralise the negative charge produced by aluminium substitution (CuCHA). Unit cell parameters are fixed to those previously optimised for all silicon Chabazite,[19] while the fractional coordinates of the atoms inside the unit cell are optimised for each structure. Moreover, frequencies are computed numerically considering only the Cu-H_2 fragment.

For comparison and in order to get a better understanding of Cu-H_2 interaction, we have also considered the interaction of H_2 with naked Cu^+ and with Cu^+ coordinated to T3 (CuZ).

Both HF[20,21] and B3LYP[22,23] have been used as levels of theory. The employed basis set has been adapted to the use in periodic calculations. For Cu a modified TVZ(P) optimised by Alhrichs and co-workers has been adopted.[24] The modification consists on removing the most diffuse s function and fixing the exponent of the second most diffuse function s function to 0.15. For H the 6-31G(d,p) basis set has been considered,[25] while for Si, Al and O we have used the same basis set as in previous periodic studies of Chabazite.[19] This basis set will be denoted hereafter BS1. In addition, BS2, is a triple-ζ plus polarization quality basis for Cu and O, and double-ζ plus polarisation quality basis for Al, Si and H. We have used the Ahlrichs's TVZ(P)[24] for Cu, VTZ(P)[26] for O and DZ(P)[26] for Al and Si while for H the Pople's 6-31G(d,p) has been used[25]). Basis set superposition error (BSSE) has been estimated using counterpoise method.[27]

Periodic calculations have been performed with CRYSTAL[28] package and non-periodic calculations with both GAUSSIAN98[29] and CRYSTAL packages.

An analysis of the adsorption energy has been performed using the partition scheme implemented in the ADF program.[30,31] As hybrid functionals are not available in ADF, the analysis has been made using the BLYP[23,32] functional at the geometries obtained with B3LYP. A triple-ζ plus polarization basis set has been used.

4.4 Results and discussion

Figure 4.1 presents the three possible sittings of Cu^+ cations in Chabazite using the nomenclature of Calligaris et al.[33] These are site I (in the 6-membered ring), site III (between two 6-membered ring) and site IV (in the 8-membered ring which connects two supercages). All three possible sittings have been considered. However, only two of them have been found to be stable for Cu^+ cations. Geometry optimization starting from Cu^+ sitting at site III evolved to Cu^+ located at site I indicating that Cu^+ is too big to be located between the 6-membered rings.

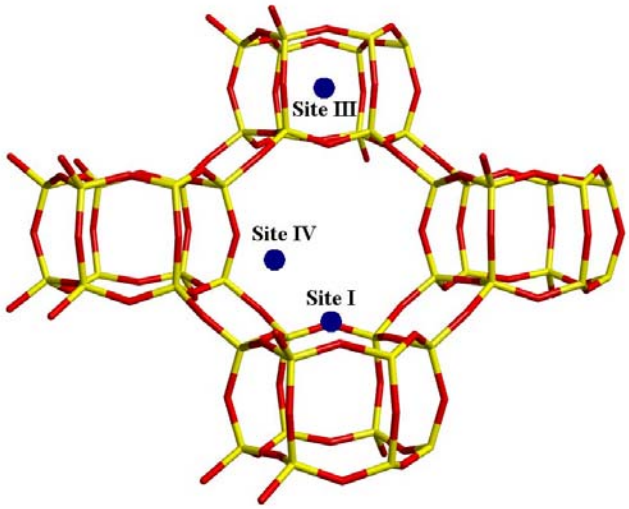

Figure 4.1 Possible sitting of Cu^+ cations in Chabazite as defined by Calligaris et al.[33]

Figure 4.2 presents the optimised geometries of CuCHA for sites I and IV and their relative stabilities. At all considered levels of theory site I is the most stable location. At this site Cu^+ coordinates to three oxygens of the 6-membered ring, those that originally were oriented to the inner part of the ring. All three Cu-O distances are different, the shorter one being that related with an oxygen bonded to aluminium. HF level leads to considerably longer Cu-O distances than B3LYP.

On the other hand, the coordination of Cu^+ at site IV takes place only through two oxygens bonded to aluminium. Cu-O distances are not equal, the shorter one being the

most distant to the 6-membered ring. As observed for site I, HF leads to longer distances than B3LYP. Site IV is only 0.8 kcal/mol less stable than site I at the HF level. However, with B3LYP this site is considerably less stable (7.9 kcal/mol). The lower stability of site IV is due to the fact that it is less saturated. The larger energy difference observed at the B3LYP level could be explained considering that Cu-O distances are shorter and CuCHA interactions stronger at this level and, thus, the loss of the third coordination is more relevant.

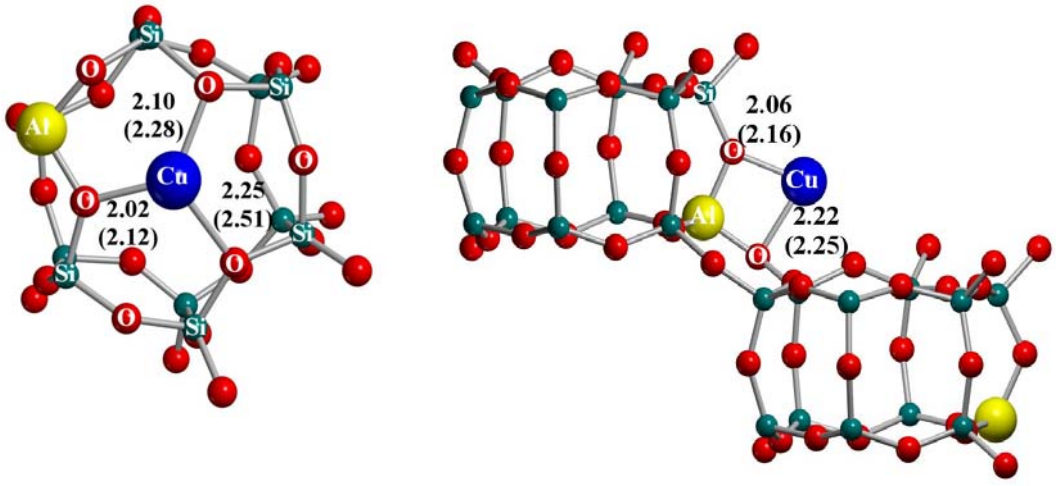

Site I	**Site IV**
0.0 (0.0)	7.9 (0.8)

Figure 4.2 B3LYP (HF) optimised structures and stabilities of CuCHA. Distances in Å

The present results agree with the experiments done by Dědeček et al.[34] which showed that Cu^+ cations are located only at sites IV and I. However, some discrepancies should be pointed out: their results indicate that at low Cu^+ loadings only site IV was populated while according to our results site I is more stable. The observed differences might be attributed to some factors not considered here such as diffusion.

Adsorption of H_2 in copper exchanged Chabazite can take place at the above reported positions. Figure 4.3 shows the optimised geometries of H_2-CuCHA at both sites and Table 4.1 presents the H_2 adsorption energy, H-H stretching red shift and Mulliken population analysis. At the HF level, adsorption of H_2 at the most stable site I is not

favourable and the optimisation spontaneously evolved to dissociation. On the other hand, the adsorption energy of H_2 at the less saturated site IV is −1.0 kcal/mol.

At the B3LYP level, molecular hydrogen absorbs at both Cu^+ sites. The strongest adsorption is observed at the less saturated site IV. At this position the coordination of H_2 takes place through a side-on structure in the O-Cu-O plane. Cu-H distances are 1.65 Å, notably shorter than those obtained at the HF level. The H-H bond length increases from 0.742 up to 0.802 Å and the red shift is 957 cm^{-1}. The computed H_2 adsorption energy at this site is -13.4 kcal/mol.

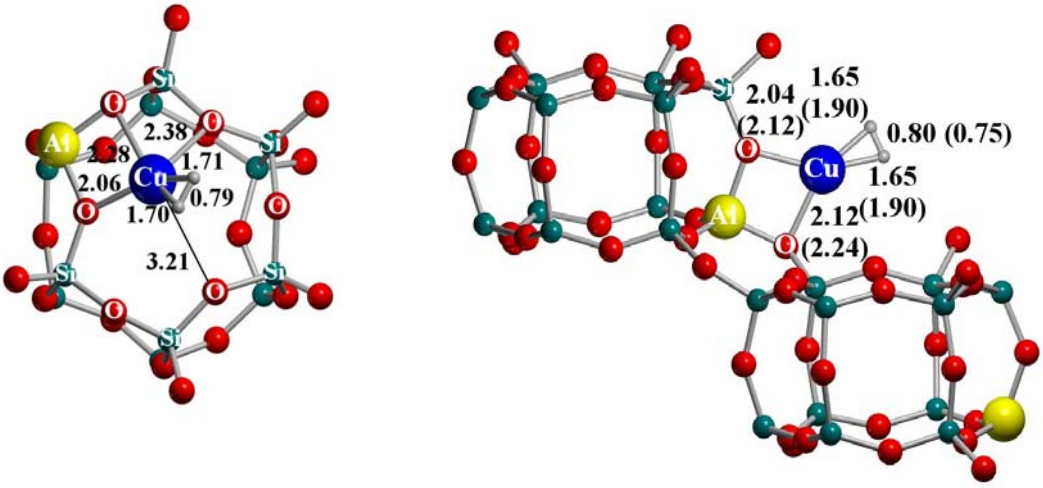

Site I **Site IV**

Figure 4.3 B3LYP (HF) optimised structures of H_2-CuCHA. Distances in Å

Table 4.1 H_2 adsorption energies, H-H stretching red shift and Mulliken population analysis for B3LYP periodic calculation approach in all stable sittings of Cu^+ cations

			Mulliken Charges	
Site	E_{ads} [a]	$\Delta\nu$ [b]	Cu	H_2
Site I	−4.4 (−3.1)	847	0.41	0.13
Site IV	−16.0 (−13.4)	957 *(964)*	0.40	0.14

[a] In kcal/mol. In parenthesis counterpoise corrected value
[b] In cm^{-1}. Values in parenthesis include anharmonic correction

If the anharmonic correction is included the red shift increases up to 964 cm^{-1}. This anharmonicity is computed evaluating the energy of the systems at different H-H distances, obtained by a symmetric shortening or elongation around the H-H distance of the minimum (from 0.402 to 1.402 Å). The obtained values are fitted to a sixth degree polynomial function, which is used to solve the one-dimensional nuclear Schrödinger equation to obtain the first three vibrational states, from which the anharmonic correction can be obtained. The nuclear Schrödinger equation has been solved using the program ANHARM.[35]

The coordination at site I is much less favourable (adsorption energy -3.1 kcal/mol). Optimised geometry of H_2-CuCHA at this site shows that Cu-H distances are longer than those obtained for site IV and the elongation of H-H bond is smaller, in agreement with the smaller interaction energy. Moreover, in order to interact with H_2, Cu^+ moves out of the plane of the six membered ring, loses the interaction with the most distant oxygen and decreases the interaction with the other two oxygens. This great geometry reorganisation can be understood if one considers that the preferred coordination of H_2 takes place in the same plane defined by Cu^+ and zeolite oxygens. Thus, as Cu^+ cation in the 6-membered ring interacts with three oxygens in the same plane (see Figure 4.2), there is no space left for the adsorption of H_2 and an important reorganisation is needed. As expected, the computed red shift of H_2 adsorbed at site I (847 cm^{-1}) is smaller than that obtained for site IV. However, considering the much weaker H_2-CuCHA interaction at this site the red shift is still significant.

IR experimental data for the adsorption of H_2 on CuZSM-5 and CuY are available.[4] For CuZSM-5 at low temperatures a weak band at 3079 cm^{-1} is observed, which is attributed to molecular hydrogen interacting with Cu^+. The effect of increasing the temperature decreases the band height, but it is still clearly observed at 300 K, indicating that the adsorption must be quite strong. The experimental red shift is 1081 cm^{-1}. However, this band is not observed when H_2 is adsorbed on CuY. This different behaviour can be understood considering the sitting sites of Cu^+ in the two zeolites. Both experimental and theoretical studies agree that CuZSM-5 zeolite presents two different Cu^+ sites,[13,14,36-38] one highly coordinated and another only coordinated to two oxygens. These sites present similar environments to those found for our Chabazite model (sites I and IV). The computed H-H red shift of H_2 interacting with the most active Cu^+, site IV,

(964 cm^{-1}) is quite similar to that measured experimentally (1081 cm^{-1}). Thus, this agreement indicates that Cu^+ ions coordinated to two oxygens in CuZSM-5 are the ones responsible for the H_2 absorption observed at room temperature, whereas, high saturated Cu^+ cations would remain mainly inactive, as the adsorption energy is weak and also entropic effects would destabilise this adsorption. In contrast, CuY zeolite only presents highly coordinated Cu^+ cations in the 6-membered ring[36,39,40] and so, according to our calculations for site I, the H_2 adsorption would not be so favourable, so that the absence of the H-H band can be explained.

The above-mentioned results clearly indicate that the agreement with experiments is much better for B3LYP than for HF results, which points out the importance of electron correlation for treating these systems. The same conclusion had been obtained for Cu-H_2^+ and other Cu^+-L systems.[6,7] Consequently, these results illustrate the great importance of one of the latest improvements of CRYSTAL code: the inclusion of DFT methods.

In order to get a better understanding of the Cu^+-H_2 interaction and to analyse the effect of increasing the basis set we have studied the coordination of H_2 to Cu^+ and to the CuZ (T3) cluster at the B3LYP level of calculation. It must be pointed out that with the tritetrahedral [$H_3SiOAl(OH)_2OSiH_3$] cluster, Cu^+ ions can only coordinate to two oxygens, so that only site IV can be modelled. Figure 4.4 presents the optimised structures of Cu^+–H_2, CuZ and (H_2)CuZ. The results obtained for these systems and for H_2-CuCHA are presented in Table 4.2. Figure 4.5 presents the CuZ orbitals involved in the interaction with H_2. $3d_\sigma$ and 4s can interact with the σ_g orbital of H_2 and $3d_\pi$ orbital corresponds to the 3d Cu orbital which can interact with the σ_u orbital of H_2.

For Cu^+-H_2 and (H_2)CuZ the results obtained with BS1 and BS2 basis sets are very similar. Moreover, the inclusion of zero-point corrections leads to a D_0 bond dissociation energy of 14.3 kcal/mol for Cu^+-H_2, in excellent agreement with previous theoretical results (D_0= 16.6 [6] or 13.8[7] kcal/mol) and also with the experimental value (D_0= 15.4 kcal/mol).[6] Consequently, it is expected that periodic results obtained with BS1 would be accurate enough.

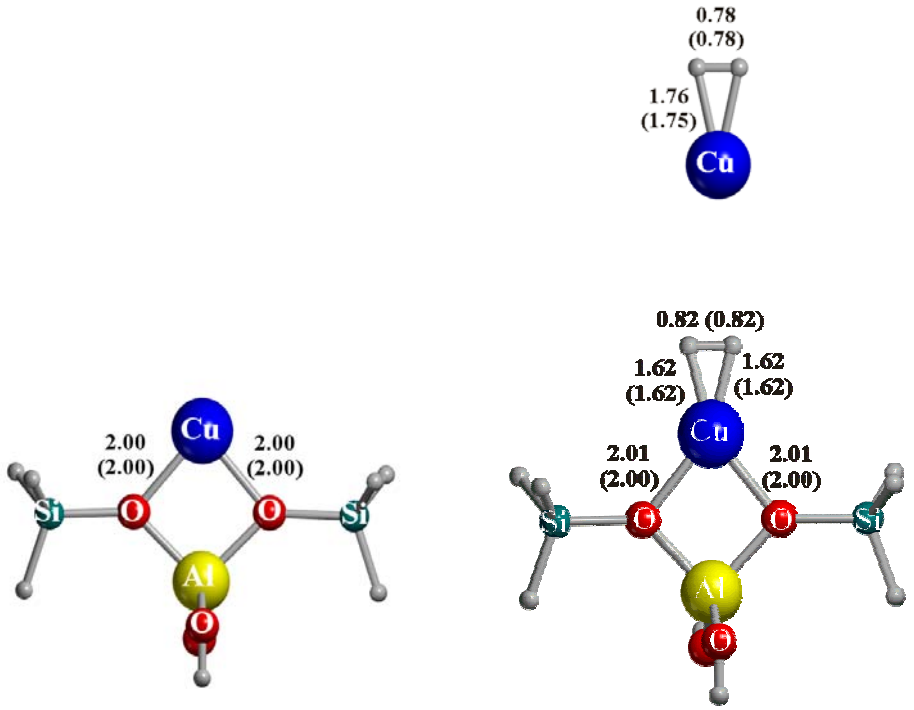

Figure 4.4 B3LYP/BS2 (B3LYP/BS1) optimised structures for Cu^+-H_2 and $(H_2)CuZ$ systems

Table 4.2 H_2 adsorption energy[a], H-H stretching red-shift (cm^{-1}) and population analysis obtained at B3LYP level in Cu^+-H_2, $(H_2)CuZ$ cluster and periodic H_2-CuCHA

				Population analysis[b]					
				Charge		Occupation			
System	Basis	E_{ads}[a]	Δν	Cu	H_2	4s	$3d_\sigma$	$3d_\pi$	$3d_{tot}$
$Cu\text{-}H_2^+$	BS1	−16.8(−16.4)	629	0.97/*0.73*	0.03/*0.27*	0.06	2.00	2.00	10.00
	BS1(C)[c]	−16.7							
	BS2	−16.5(−16.0)	624	0.96/*0.75*	0.04/*0.25*	0.08	1.98	1.97	9.95
$(H_2)CuZ$	BS1	−17.5(−16.4)	1207	0.86/*0.41*	-0.05/*0.10*	0.23	1.96	1.88	9.84
	BS1(C)[c]	−17.8							
	BS2	−17.6(−16.2)	1129	0.90/*0.39*	-0.02/*0.14*	0.25	1.95	1.89	9.84
H_2-CuCHA	BS1	−16.0(−13.4)	957	*0.40*	*0.14*				

[a] In kcal/mol. In parenthesis adsorption energy after counterpoise correction
[b] Natural population analysis, in italic Mulliken population analysis
[c] Calculation performed using CRYSTAL package.

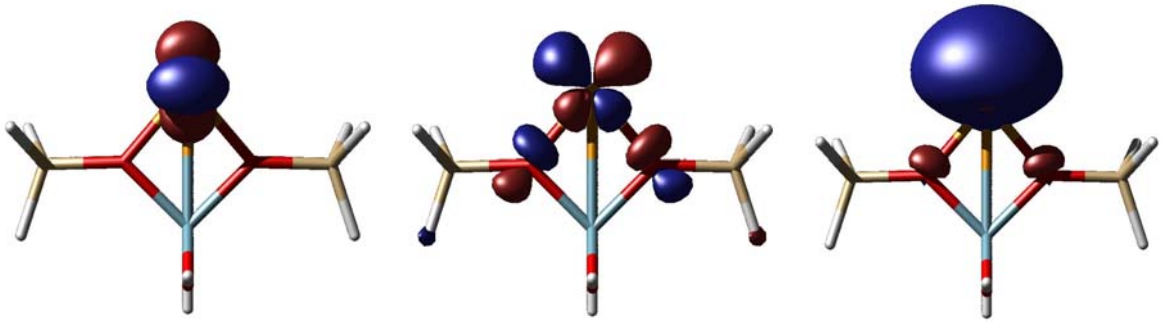

$3d_\sigma$ **$3d_\pi$** **4s**

Figure 4.5 Orbitals of CuZ fragment involved in the interaction with H_2

Results obtained for (H_2)CuZ and H_2-CuCHA are quite similar (see Figures 4.3 and 4.4), the most significant difference being the H-H distance. Moreover, comparing Cu^+-H_2 with H_2-CuCHA or (H_2)CuZ is clearly observed that the inclusion of the zeolite produces an important increase of the H-H distance as well as a shortening of the Cu-H distances. These differences suggest that the Cu^+-H_2 interaction in the zeolite should be stronger than in gas phase. However, the H_2 adsorption energy for both systems is very similar.

To get a deeper insight, the H_2 adsorption energies to Cu^+ and the CuZ cluster have been decomposed using the Extended Transition State[41,42] implemented in the ADF program. As hybrid functionals are not available in ADF, the analysis has been made using the BLYP functional at the geometries obtained with B3LYP. A triple-ζ plus polarization basis set has been used. The energy has been decomposed in the following terms:

$$E_{ads}=E_{prep}+E_{Pauli}+E_{elstat}+E_{orb}$$

E_{prep} is the preparation energy associated to the geometry distortion of H_2 and CuZ in the formation of (H_2)CuZ. E_{Pauli} is associated to closed shell repulsions between fragments. E_{elstat} is the electrostatic interaction energy arising from the interaction between both fragments, each fragment having the electron density that it would have in the absence of the other fragment. E_{orb} is the orbital interaction term that arises when the electron densities of both fragments are allowed to relax and accounts for charge transfer

and polarization. By selectively deleting fragment virtual orbitals, we have decomposed this term into three contributions:

$$E_{orb}=E_{don}+E_{back}+E_{pol}$$

E_{don} is the energy stabilization obtained when only the first virtual orbital of the metal fragment is included and comes from the electron donation from the occupied σ_g orbital of H_2 to 4s of Cu^+. E_{back} is associated to the back-donation from the occupied $3d_\pi$ orbital of Cu^+ to σ_u of H_2. Finally, E_{pol} is the additional stabilization gained when all virtual orbitals are included and can be associated to the polarization of both fragments.

The results are summarized in Table 4.3. We have also considered two additional clusters generated from the results of the periodic calculations and representing sites IV (CuZ_{SiteIV}) and I (CuZ_{SiteI}) of CuCHA. CuZ_{SiteIV} is equivalent to CuZ but with a different geometry, while cluster CuZ_{SiteI} contains Cu^+ in a six-membered ring $[AlSi_5O_8H_{12}]$. Figure 4.6 presents these clusters.

Table 4.3 Analysis[a] of the adsorption energy, using BLYP level of theory

		Cu^+-H_2-	$(H_2)CuZ$	$(H_2)CuZ_{siteIV}$	$(H_2)CuZ_{siteI}$
prep		+2.9	+4.5	+5.8	+7.8
Pauli		+35.9	+64.9	+56.7	+58.2
elstat		–30.0	–51.6	–45.8	–44.3
orb		–27.1	–35.3	–31.8	–29.1
	don	–9.4	–8.6	–8.2	–9.2
	back	–0.8	–4.8	–3.9	–3.7
	pol	–16.9	–21.9	–19.7	–16.2
E_{ads}		-18.3	-17.5	-15.1	-7.4

[a] See text for definitions. In kcal/mol

The adsorption energies for Cu^+ and CuZ are similar to the values obtained at the B3LYP level of calculation (see Table 4.2). Moreover, the values obtained for the CuZ_{SiteIV} and CuZ_{SiteI} clusters follow the same trends computed from the periodic calculations for adsorptions on sites IV and I, respectively (see Table 4.1).

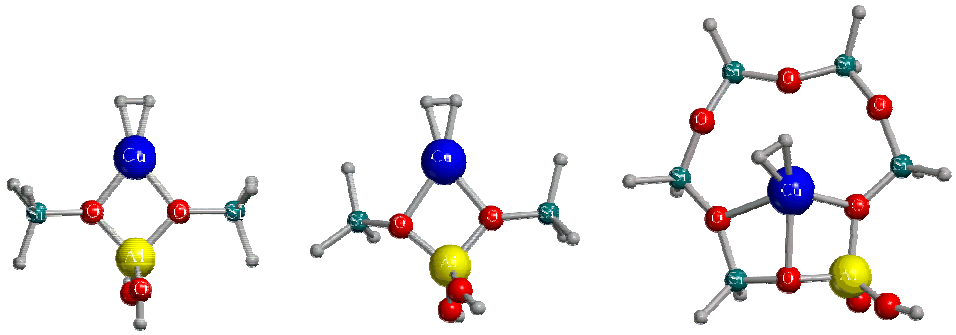

$(H_2)CuZ$ $(H_2)CuZ_{siteIV}$ $(H_2)CuZ_{siteI}$

Figure 4.6 Clusters considered in the decomposition of the adsorption energy

Let us compare the results obtained for Cu^+ and CuZ. The adsorption energies are very similar. However, the contribution of each term differs from one case to another. The preparation energy is larger for CuZ since it involves a distortion of the CuZ cluster and the H-H bond is more elongated than for Cu^+-H_2. The Pauli repulsion is also larger for CuZ, since the Cu-H distances are notably shorter (see Figure 4.4). This repulsion is partly compensated by the electrostatic term that is more stabilizing for CuZ. However, the sum of Pauli and electrostatic contributions is still repulsive. So, electrostatics is not enough to understand the adsorption process.

In both cases the orbital interaction term is stabilizing enough to make adsorption energetically favourable. The magnitude of this term can also be related to the Cu-H_2 distance, so that the stabilization is larger for CuZ than for Cu^+. In both cases polarization accounts for about 62 % of the stabilization. However, there are significant differences in the relative weight of the donation and back-donation contributions. For Cu^+-H_2 back-donation is only 8.5% of the donation term, whereas for $(H_2)CuZ$ this contribution increases up to 56%. These differences are due to the effect of the zeolite cluster, which polarizes the $3d_\pi$ orbital of Cu^+ (see Figure 4.5), through mixing with one of the 4p orbitals of Cu. This polarization reduces the repulsion between Cu^+ and the zeolite framework, and at the same time favours the charge transfer from Cu^+ to σ_u of H_2. Consequently, the H-H bond length and the red-shift increase. The increase of back-donation is also observed when one analyses the Cu^+ populations (Table 4.2). Comparing

Cu^+-H_2 with $(H_2)CuZ$ it is clearly observed that the population of the $3d_\pi$ orbital decreases considerably for $(H_2)CuZ$.

The results obtained for CuZ_{SiteIV} are roughly similar to those of CuZ, the main differences being due to the variation on the Cu-H distances (see Figures 4.3 and 4.4). Moreover, the preparation energy of the CuZ_{SiteIV} cluster is larger than that of the CuZ cluster.

Comparing CuZ_{SiteIV} and CuZ_{SiteI} clusters, we can observe that for the latter the preparation energy is larger, even if the hydrogen molecule is notably less distorted. As we have already shown, H_2 adsorption at site I Cu^+ requires a large geometry reorganization. The sum of Pauli and electrostatic energies is more repulsive for CuZ_{SiteI} than for CuZ_{SiteIV}. This difference is not related to the Cu-H distances, but to the fact that the environments of H_2 in these two clusters are notably different. In particular, for CuZ_{SiteI} the adsorbed hydrogen molecule is relatively close to 6 oxygens (O-H distances between 3 and 4.1 Å), whereas for CuZ_{SiteIV} there are only two oxygens at O-H distances lower than 5.3 Å. Finally, the orbital interaction term is also less stabilizing for CuZ_{SiteI} than for CuZ_{SiteIV}. All these contributions lead to a less favourable adsorption at CuZ_{SiteI}. However, as the back-donation in CuZ_{SiteIV} and Cu Z_{SiteI} are very similar the H-H elongation is similar and also the red shift. Again this demonstrates that the back-donation is the main responsible for the H-H elongation.

Comparing $(H_2)CuZ_{SiteIV}$ with CuZ it is observed that the adsorption is more favourable by 1.4 kcal/mol for the later. Although we are not using the same functional and basis set, this difference is almost equal to that obtained between H_2-CuCHA and $(H_2)CuZ$ at the B3LYP level which indicates that the whole zeolite framework disfavours the H_2 adsorption mainly due to a mechanical constrain.

4.5 Concluding remarks.

HF and B3LYP periodic calculations using a localized basis set based on a Gaussian expansion of crystalline orbitals have been performed to study the sites of Cu^+ on Chabazite and the adsorption of molecular hydrogen. Two possible sittings of Cu^+ cations have been found to be stable: Site I, in the 6-membered ring, and site IV, in the 8-

membered ring. Cu^+ at site I coordinates to three different oxygens while Cu^+ cations at site IV are less saturated, only coordinated to two framework oxygens. Results indicate that Cu^+ located at site I is more stable than Cu^+ at site IV by 7.9 kcal/mol. These results agree well with available experimental data which indicate that sites I and IV are the only copper populated sites in Chabazite.[34]

H_2 adsorption is more favourable at site IV (-13.4 kcal/mol) than at site I (-3.1 kcal/mol). The computed harmonic red shifts are 957 and 847 cm^{-1} respectively. Including anharmonic corrections for H_2 adsorption at site IV leads to a red-shift of 964 cm^{-1} in good agreement with experimental results (1081 cm^{-1}) for H_2 adsorbed in CuZSM5. Moreover our results can be taken as a model for other zeolite frameworks to explain the IR experimental data for CuZSM-5 and CuY. The less saturated sites on CuZSM-5 would be those responsible of the adsorption of H_2. On the other hand, CuY only presents highly coordinated sites and no adsorption is experimentally observed.

The zeolite framework oxygen atoms coordinated to Cu^+ cations induce a polarization of the $3d_\pi$ orbital of copper in order to reduce the zeolite-Cu repulsion. This polarization favours the metal-H_2 back-donation, which is the main responsible of the H-H elongation and large red shift.

The present study demonstrates the great importance of periodic approach calculations to analyse the different sites of Cu^+ cations, evaluate their stability and the subsequent adsorption of H_2. The implementation of DFT is also essential to treat more complex systems such as transition metal exchanged zeolites where electron correlation is necessary.

The adsorption energy computed for Cu^+ exchanged Chabazite (-13.4 kcal/mol) is much larger than the one measured for alkali metal exchanged ZSM-5.[3] This fact confirms that Cu^+ exchanged zeolites may be useful for hydrogen storage.

References

(1) Dyer, A. Zeolites. In *Encyclopedia of Inorganic Chemistry*; King, R. B., Ed.; John Wiley and Sons: Chichester, 1994; Vol. 8; pp 4363.

(2) Nijkamp, M. G.; Raaymakers, J. E. M. J.; van Dillen, A. J.; de Jong, K. P. *Appl. Phys. A* **2001**, *72*, 619.

(3) Otero-Areán, C.; Manoilova, O. V.; Bonelli, B.; Rodríguez-Delgado, M.; Turnes-Palomino, G.; Garrone, E. *Chem. Phys. Lett.* **2003**, *370*, 631.

(4) Gribov, E.; Spoto, G.; Zecchina A. personal comunication

(5) Niu, J.; Rao, B. K.; Jena, P.; Manninen, M. *Phys. Rev. B* **1995**, *51*, 4475.

(6) Kemper, P. R.; Weis, P.; Bowers, M. T.; Maître, P. *J. Am. Chem. Soc.* **1998**, *120*, 13494.

(7) Maître, P.; Bauschlisher, C. W. *J. Phys. Chem.* **1993**, *97*, 11912.

(8) Aldridge, S.; Downs, A. J. *Chem. Rev.* **2001**, *101*, 3305.

(9) Weis, P.; Kemper, P. R.; Bowers, M. T. *J. Phys. Chem. A* **1997**, *101*, 2809.

(10) Bushnell, J. E.; Kemper, P. R.; Bowers, M. T. *J. Phys. Chem.* **1994**, *98*, 2044.

(11) Maseras, F.; Lledós, A.; Clot, E.; Eisenstein, O. *Chem. Rev.* **2000**, *100*, 601.

(12) Armor, J. N. *Micropor. and Mesopor. Mater.* **1998**, *22*, 451.

(13) Nachtigallová, D.; Nachtigall, P.; Sierka, M.; Sauer, J. *Phys. Chem. Chem. Phys.* **1999**, *1*, 2019.

(14) Nachtigall, P.; Nachtigallová, D.; Sauer, J. *J. Phys. Chem. B* **2000**, *104*, 1738.

(15) Treesukol, P.; Limtrakul, J.; Truong, T. N. *J. Phys. Chem. B* **2001**, *105*, 2421.

(16) Trout, B. L.; Chakraborty, A. K.; Bell, A. T. *J. Phys. Chem.* **1996**, *100*, 4173.

(17) Blint, R. J. *J. Phys. Chem.* **1996**, *100*, 19518.

(18) Dent, L. S.; Smith, J. V. *Nature* **1958**, *181*, 1794.

(19) Pascale, F.; Ugliengo, P.; Civalleri, B.; Orlando, R.; D'Arco, P.; Dovesi, R. *J. Chem. Phys.* **2002**, *117*, 5337.

(20) Hartree, D. R. *Proc. Cambridge Phil. Soc.* **1928**, *24*, 89.

(21) Fock, V. *Z. Physik* **1930**, *61*, 126.

(22) Becke, A. D. *J. Chem. Phys.* **1993**, *98*, 5648.

(23) Lee, C.; Yang, W.; Parr, R. G. *Phys. Rev. B* **1988**, *37*, 785.

(24) Schäfer, A.; Huber, C.; Ahlrichs, R. *J. Chem. Phys.* **1994**, *100*, 5829.

(25) Hehre, W. J.; Ditchfield, R.; Pople, J. A. *J. Chem. Phys.* **1972**, *56*, 2257.

(26) Schäfer, A.; Horn, H.; Ahlrichs, R. *J. Chem. Phys.* **1992**, *97*.

(27) Boys, S. F.; Bernardi, F. *Mol. Phys.* **1970**, *19*, 553.

(28) Saunders, V. R., Dovesi, R.; Roetti, C.; Orlando, R.; Zicovich-Wilson, C. M.; Harrison, N. M.; Doll, K.; Civalleri, B.; Bush, I. J.; D'Arco, Ph.; Llunell, M. CRYSTAL03 development version

(29) Frisch, M. J.; Trucks, G. W.; Schlegel, H. B.; Scuseria, G. E.; Robb, M. A.; Cheeseman, J. R.; Zakrzewski, V. G.; Montgomery, J. A.; Stratmann, R. E.; Burant, J. C.; Dapprich, S.; Millam, J. M.; Daniels, A. D.; Kudin, K. N.; Strain, M. C.; Farkas, O.; Tomasi, J.; Barone, V.; Cossi, M.; Cammi, R.; Mennucci, B.; Pomelli, C.; Adamo, C.; Clifford, S.; Ochterski, J.; Petersson, G. A.; Ayala, P. Y.; Cui, Q.; Morokuma, K.; Malick, D. K.; Rabuck, A. D.; Raghavachari, K.; Foresman, J. B.; Cioslowski, J.; Ortiz, J. V.; Baboul, A. G.; Stefanov, B. B.; Liu, G.; Liashenko, A.; Piskorz, P.; Komaromi, I.; Gomperts, R.; Martin, R. L.; Fox, D. J.; Keith, T.; Al-Laham, M. A.; Peng, C. Y.; Nanayakkara, A.; Gonzalez, C.; Challacombe, M.; Gill, P. M. W.; Johnson, B. G.; Chen, W.; Wong, M. W.; Andres, J. L.; Head-Gordon, M.; Replogle, E. S.; Pople, J. A. Gaussian 98; Gaussian Inc.: Pittsburgh, 1998.

(30) ADF 2002.03, SCM, Theoretical Chemistry, Vrije Universiteit, Amsterdam, The Netherlands.

(31) te Velde, G.; Bickelhaupt, F. M.; Baerends, E. J.; Fonseca-Guerra, C.; van Gisbergen, S.; Snijders, J. G.; Ziegler, T. *J. Comput. Chem.* **2001**, *22*, 931.

(32) Becke, A. D. *Phys. Rev. A* **1988**, *38*, 3098.

(33) Calligaris, M.; Nardin, G.; Randaccio, L. *Zeolites* **1984**, *4*, 251.

(34) Dědeček, J.; Wichterlová, B.; Kubát, P. *Micropor. and Mesopor. Mater.* **1999**, *32*, 63.

(35) Ugliengo, P. ANHARM-A program to solve monodimensional nuclear Schrödinger equation, 1989, unpublished.

(36) Dědeček, J.; Sobalík, Z.; Tvarůžková, Z.; Kaucký, D.; Wichterlová, B. *J. Phys. Chem.* **1995**, *99*, 16327.

(37) Lamberti, C.; Bordiga, S.; Salvalaggio, M.; Spoto, G.; Zecchina, A.; Geobaldo, F.; Vlaic, G.; Bellatreccia, M. *J. Phys. Chem. B* **1997**, *101*, 344.

(38) Yamashita, H.; Matsuoka, M.; Tsuji, K.; Shioya, Y.; Anpo, M.; Che, M. *J. Phys. Chem.* **1996**, *100*, 397.

(39) Lamberti, C.; Spoto, G.; Scarano, D.; Pazé, C.; Salvalaggio, M.; Bordiga, S.; Zecchina, A.; Turnes-Palomino, G.; D'Acapito, F. *Chem. Phys. Lett.* **1997**, *269*, 500.

(40) Turnes-Palomino, G.; Bordiga, S.; Zecchina, A.; Marra, G. L.; Lamberti, C. *J. Phys. Chem. B* **2000**, *104*, 8641.

(41) Ziegler, T.; Rauk, A. *Theor. Chim. Acta* **1977**, *46*, 1.

(42) Ziegler, T.; Rauk, A. *Inorg. Chem.* **1979**, *18*, 1558.

5. Keto-enol isomerization in HZSM-5

5.1 Introduction

The aldol condensation is a very important reaction in organic synthesis. This reaction takes place between two molecules which present a carbonyl group (aldehydes and/or ketones) and involves two steps:[1] 1) the formation of an enol or enolate form and 2) reaction of that enol/enolate with the carbonyl group of the other molecule, forming a new C-C bond. Normally the obtained aldol product loses a water molecule to lead to the α,β-unsaturated carbonyl. The simplest aldol condensation involves one acetaldehyde and one formaldehyde molecule and it is represented in scheme 5.1. It has been observed that aldol condensation can be catalysed by both acids and basis.[1] Since zeolites present high acidity it has been thought that they could be good catalysts for this process and, nowadays, several published articles announce the great catalytic activity of several acidic zeolites, especially HZSM-5.[2-9] The importance of this reaction in chemical industry has led several companies to register patents related with this process.[10,11]

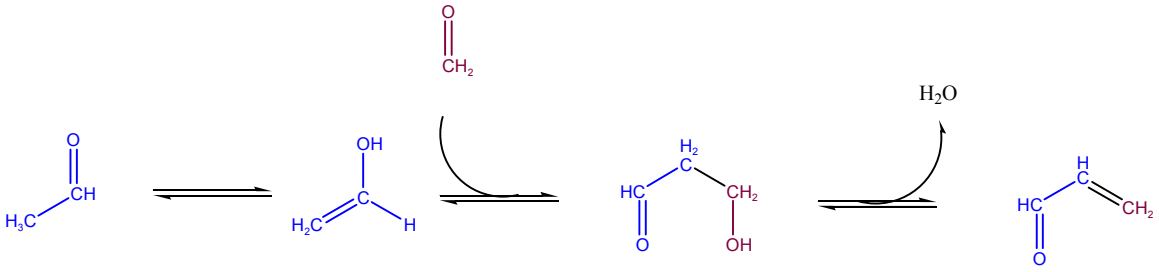

Scheme 5.1 Aldol condensation mechanism

The nature of adsorbed acetaldehyde and ketones on different zeolites has been studied by means of infrared spectroscopy,[3,5,12] NMR[6,7,13] and theoretical calculations.[12-14] However, to our knowledge, the heat of adsorption of aldehydes and ketones on zeolites has only been measured for acetone.[3,13] On the other hand, the factors that control the catalytic activity of the aldol condensation have also been discussed in experimental studies.[3,6,8] One of the most important factors is suggested to be the acidity of the zeolite. The proposed mechanism for the aldol condensation in zeolites assumes that the first step is the keto-enol isomerization. In a second step the enol reacts with an aldehyde molecule that is coordinated to an acid site of the zeolite (Scheme 5.2).[3,5,8]

Thus, the formation of the enol form of the aldehyde molecule, through a keto-enol isomerization, is a very important reaction in the aldol condensation. In fact, previous gas-phase studies have shown that this step is the crucial and rate determinant one.[15]

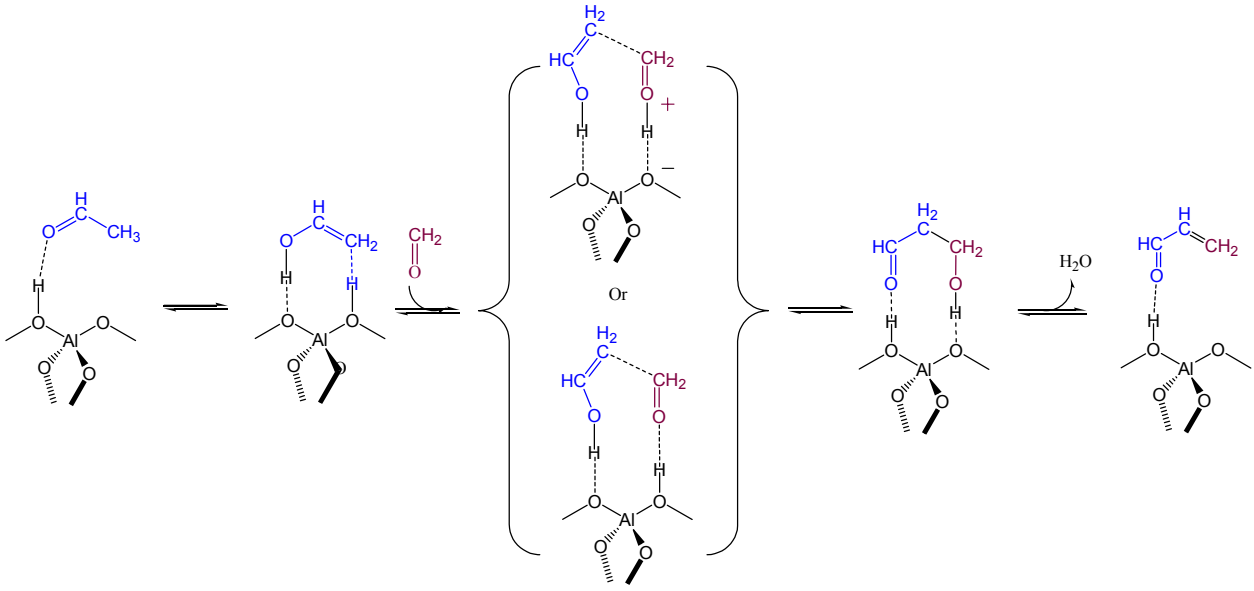

Scheme 5.2 Postulated mechanism of aldol condensation in zeolites

The keto-enol isomerization of acetaldehyde in the gas phase and catalysed by a solvent molecule has recently been studied in our group.[16] Results show that in gas phase the reaction is endothermic and presents a very high-energy barrier (67.9 kcal/mol). Although a water molecule produce an important catalytic effect, the energy barrier of the keto-enol isomerization is still high (40.6 kcal/mol). The catalytic effect of the solvent molecule is due to the formation of hydrogen bonds that contribute to stabilize the transition state structure and to a smaller geometry distortion of acetaldehyde along the process.

Zeolites present acidic and basic sites close enough to each other to exhibit bifunctional catalysis. On the other hand, because geometry distortions of acetaldehyde during the isomerization reaction are expected to be smaller in proton-exchanged zeolites than in the solvent-assisted process, the catalysis by zeolites might be more efficient.

To our knowledge, no theoretical study related to the keto-enol isomerization in proton-exchanged zeolites or any possible step of the aldol condensation in zeolites has been reported.

5.2 Goal

The aim of the present chapter is to study the catalytic activity of HZSM-5 in the keto-enol isomerization of acetaldehyde. The obtained results are compared with those available in the literature for the reaction in gas phase or catalysed by a single water molecule. Moreover, the effect of the zeolite framework around the Brønsted acid site is also analysed by enlarging the cluster size using the ONIOM approach.[17-19] The behaviour of different ONIOM level combinations is also analysed.

5.3 Computational details

Three different clusters have been used to model the zeolite and they are schematically represented in Figure 5.1. The simplest model (T3) consists on a tritetrahedral [$H_3SiOAl(OH)_2OSiH_3$] cluster. This cluster has been used in the previous chapters for Cu exchanged zeolites and has been shown to provide similar results to those obtained with periodic calculations and with the QM-Pot[20,21] scheme.[22] Cu^+ substitution by H^+ produces a more flexible cluster as H^+ is only bonded to one oxygen atom. This higher flexibility can lead to unrealistic structures, in which the terminal OH groups interact with the adsorbed molecule. Thus aluminium, both silicon and the oxygen atoms between them have been fixed to lie in the same plane. Moreover, we have also performed calculations using a pentatetrahedral [$(H_3SiO)_4Al$] cluster (T5) to represent the active site of the zeolite. Such cluster avoids the unrealistic interactions with terminal OH and so, no geometry constraints have been imposed. A larger cluster formed by 63 tetrahedra has been built to introduce the 10-membered ring, as well as several 5-membered rings to naturally constrain the structure of the zeolite. Moreover, this cluster has been enlarged around the acid site in order to get a better description of the acidic properties. As this cluster is too big to be computed at the B3LYP level, the ONIOM2

scheme has been applied. The inner layer is equal to T3 and has been represented with solid atoms in Figure 5.1. This latter cluster will be named hereafter T3:T63.

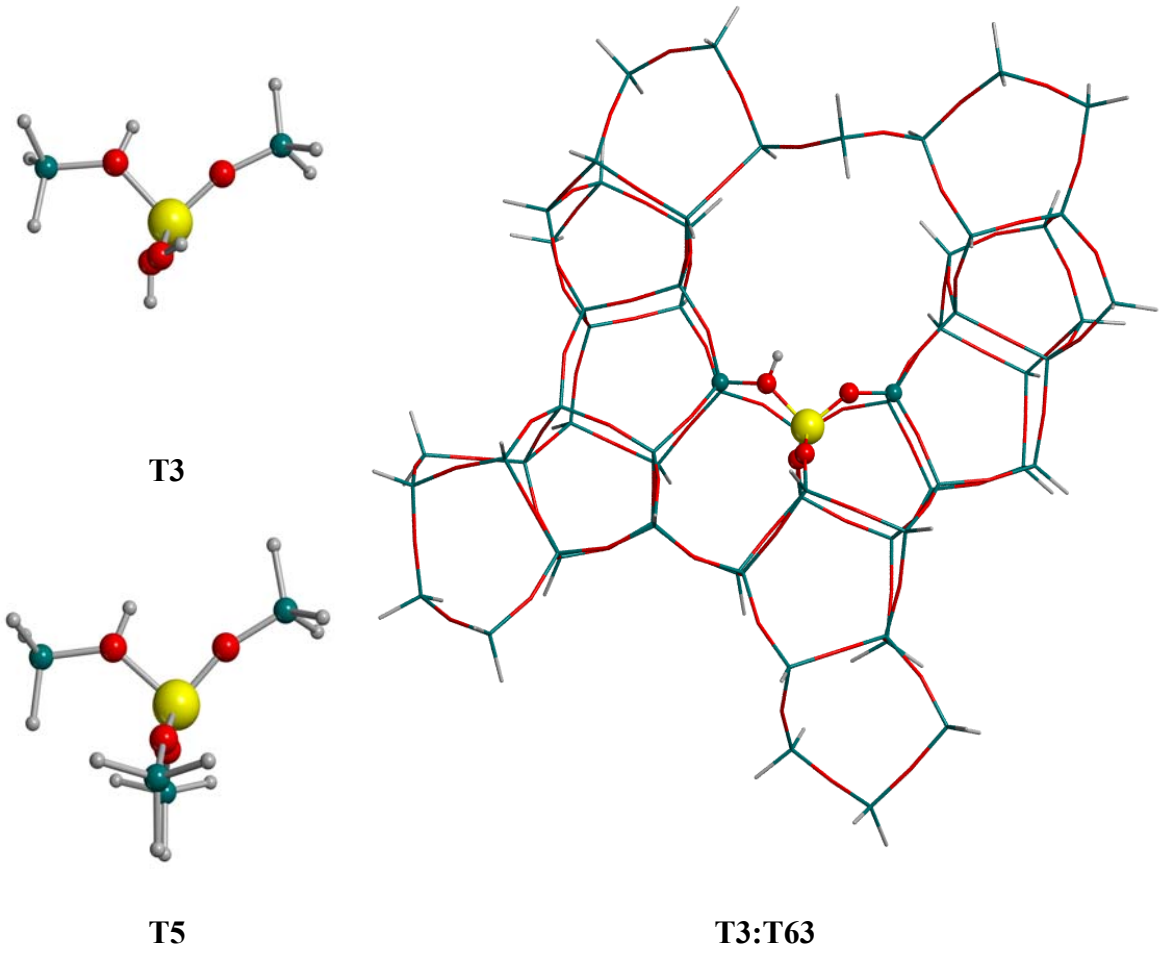

Figure 5.1 Clusters used to model the HZSM-5 zeolite. The solid atoms in T3:T63 cluster are treated at the B3LYP level.

Geometry optimisations and harmonic vibrational frequencies have been computed using B3LYP[23,24] and the 6-31++G(d,p) basis set.[25] It should be mentioned that density functional methods do not take into account the dispersion energy. However, in the present study dispersion forces are expected to be a minor component of the global interaction. To test the effect of further enlarging the basis set, we have also performed single point B3LYP calculations with the 6-311++G(2d,2p)[26,27] basis set for the stationary points localised for the T3 cluster. The results obtained show that the effect of

enlarging the basis set is small at this level of calculation, the largest variation being 1.3 kcal/mol. Because of that, we will only report the results with the smaller basis set.

Basis set superposition error has been corrected using the counterpoise procedure.[28] For the transition state structure, the counterpoise correction has been computed by assuming the same two fragments considered for the (Enol)HZ intermediate. We have chosen this partition because the geometry of the transition state structure is product-like. Thermodynamic corrections have been obtained at 298.15 K and 1 atm assuming an ideal gas, unscaled harmonic vibrational frequencies, and the rigid rotor approximation by standard statistical methods.

The inner part of T3:T63 cluster is computed at the same B3LYP/6-31++G(d,p) level of theory. For the outer layer three different levels have been considered, the semiempirical AM1[29] (B3LYP:AM1) and MNDO[30] (B3LYP:MNDO) methods and the HF/3-21G[31,32] (B3LYP:HF) level. Full T3:T63 optimisations have been performed at the B3LYP:AM1 and B3LYP:MNDO level combinations, while for HF/3-21G only single point calculations at the B3LYP:MNDO structure has been performed. We have also tested the performance of UFF[33] as low level. However during the optimisation process the system loses its zeolite structure and the 10-membered channel.

All calculations have been performed with GAUSSIAN98 package[34]

5.4 Results and discussion

5.4.1 Free cluster results.

Figure 5.2 presents the optimised structures of HZSM-5 and all the stationary points involved in the keto-enol isomerization (reactant, transition state structure and product), located with clusters T3 and T5. Since the results obtained with T3 and T5 are very similar and T3 is the cluster used as the inner part in the ONIOM2 calculations, we will mainly refer to the results obtained with T3 in the discussion. Only at the end of the present section a brief comparison with T5 results will be done.

Acetaldehyde interacts with the zeolite through a hydrogen bond between the carbonylic oxygen and the acid $-O_2H$ group of the zeolite. This hydrogen bond is nearly linear and presents a short $O_2H{-}O$ distance (1.634 Å). Consequently, the zeolitic $O_2{-}H$

distance increases considerably (from 0.968 Å to 1.004 Å) and the O_2H stretching frequency is strongly downshifted (-719 cm^{-1}).

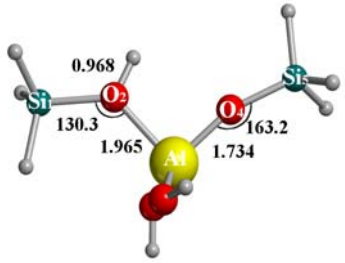

HZ T3

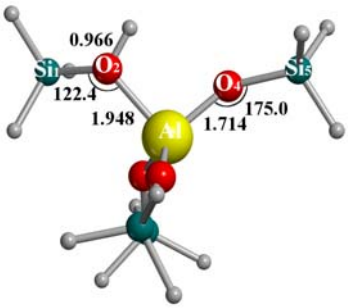

HZ T5

T3

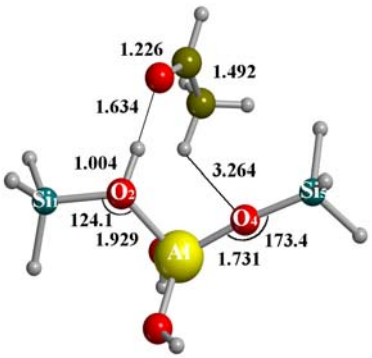

(Keto)HZ

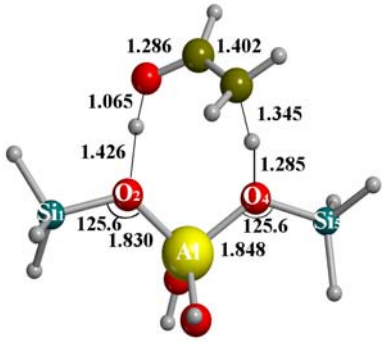

TS

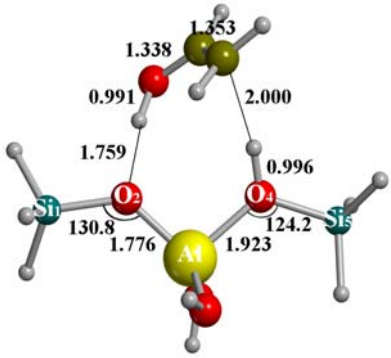

(Enol)HZ

T5

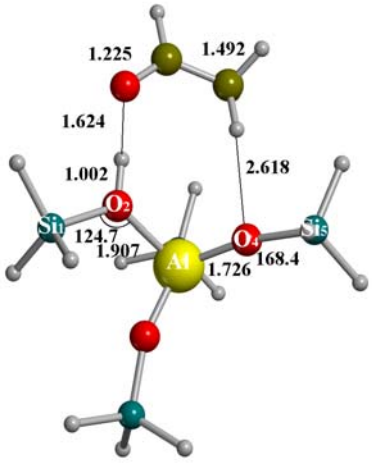

(Keto)HZ

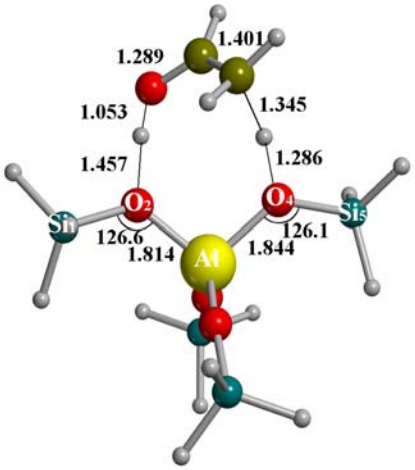

TS

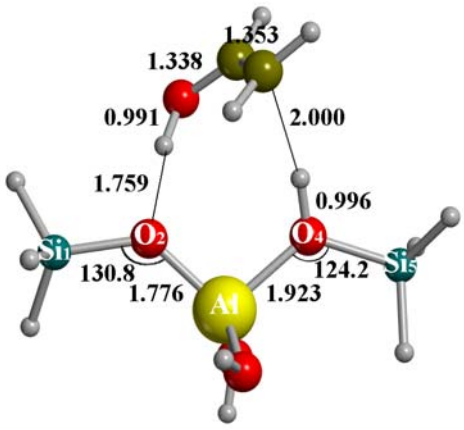

(Enol)HZ

Figure 5.2 B3LYP optimised HZ, intermediate and transition state structures of the keto-enol isomerization process using T3 and T5. Distances in Å and angles in degrees.

Zecchina and co-workers[35] have classified the adsorbed molecules in H^+ exchanged zeolites according to their proton affinity and to the strength of hydrogen bond interaction established with the zeolite as weak, medium-strong, or strong hydrogen bonds. Acetaldehyde's proton affinity lies in the range of medium-strong hydrogen bonds, which are associated with a red shift of the Brønsted site from 400 to 1000 cm^{-1}. Our computed value lies in the appropriate range. The counterpoise corrected binding energy (11.9 kcal mol^{-1}) is also consistent with the energy classification for a medium-strong hydrogen bond, since the stabilization due to the $CH–O_4$ interaction is expected to be small. This hydrogen bond interaction is similar to that determined at the MP2 level and correcting for basis set superposition error (13.9 kcal/mol). Calculations for acetone provide similar hydrogen bond interactions.[12-14] However, the experimentally determined heat of adsorption of acetone on HZSM-5 (31.1 kcal/mol)[13] is much larger than the theoretical values. This difference has been attributed to "non-local interactions"; that is, to the confinement effect due to the structure of the zeolite cavity and the interactions of polarizable framework atoms with acetone, and to the long-range electrostatic forces, which have been approximated by the heat of adsorption of acetone in silicalite (16.0 kcal/mol). T3 cluster could not account for the above-mentioned interaction and thus the comparison between experimental and computed binding energies should be done with the T3:T63 cluster where at least part of the effects are expected to be included.

On the other hand, the hydrogen bond interaction between acetaldehyde and the acid site of the zeolite produces a red shift of the C=O stretching mode. Experimental studies on adsorbed acetaldehyde on HZSM-5 provide a band at 1703 cm^{-1} which is assigned to this C=O stretching vibration.[5] This value is smaller than the one computed at the B3LYP level (1771cm^{-1}). However, if one scales the computed frequencies by 0.9614 to account for systematic errors on the calculation of the force constant and the lack of anharmonic effects,[36] one obtains a value of 1700 cm^{-1} in very good agreement with the experimental observations. Moreover, the computed shift (scaled) of 42 cm^{-1} is in very good agreement with the experimental one of 40 cm^{-1}.

Our results are in contrast to what has been suggested in the experimental study of Chavez et al.[5] which state that the primary interaction between acetaldehyde and the

zeolite surface corresponds to a proton transferred structure; that is, to an ion pair. It should be pointed out that all our attempts to optimise such structure have spontaneously evolved to the keto form of acetaldehyde. Although it is suggested in the literature that long-range effects would favour the ion pair structure,[37,38] considering the good agreement between the computed and experimental CO frequency and shifts, the observed species in the adsorption of acetaldehyde on HZSM-5 does not seem to be protonated acetaldehyde but neutral acetaldehyde. On the other hand, the shift of CO would be much larger if acetaldehyde were protonated. Gas phase calculations indicate that the frequency of CO decreases about 150 cm^{-1} upon protonation. The present results are in agreement with the experimental studies of Paukshtis et al.[39] who concluded that the formation of the ion pair is only favourable if the difference in proton affinities between the probe molecule and the zeolite is less than 85 kcal/mol. For the present system such difference is computed to be 118 kcal/mol. Furthermore, ^{13}C NMR studies of acetaldehyde adsorbed on HZSM-5 indicate that at low coverage acetaldehyde is bound to the acid site through a hydrogen bond interaction.[6]

The enol form of acetaldehyde, hydroxyethylene, interacts with the zeolite through two hydrogen bonds: one in which the enol acts as proton donor and another one in which it acts as proton acceptor. The first one occurs between the hydroxyl group and the O_2 atom of the zeolite and the second one between the acid site O_4H of the zeolite and the π system of the enol. The frequency shift of the Brønsted acid site is -594 cm^{-1}, smaller than that for the keto form. This is not surprising considering the larger hydrogen bond distances and the weaker interaction. Note that the counterpoise corrected binding energy (8.5 kcal/mol) is smaller than that obtained for the (Keto)HZ intermediate even though it accounts for two hydrogen bond interactions.

The structure of the transition state is also shown in Figure 5.2. It can be observed that its geometry is closer to the product than to the reactant, as should be expected for an endothermic reaction (see below). The alcohol is nearly formed while the other proton lies half way between the C and O_4. Moreover, the zeolite presents some reorganization. The main changes correspond to the Al_3-O_2 and Al_3-O_4 distances, those related with the catalytic process, and to the $Al_3O_4Si_5$ angle. The Al_3-O_2 distance decreases 0.099 Å while the Al_3-O_4 distance increases around 0.117 Å. Consequently, in the transition state structure both distances are similar. The $Al_3O_4Si_5$ angle decreases 47.8 degrees. It should

be noted that this important change on the $Al_3O_4Si_5$ angle is due to the fact that the mechanical embedding is not considered in these cluster calculations.

Figure 5.3 shows the energetics of the keto-enol isomerization in gas phase, catalysed by a water molecule and inside the zeolite using clusters T3 and T5. The gas phase and water catalysed results have been taken from a previous study in our laboratory.[16] It should be noted that the basis set used in that study was not the same as the one used in the present work. This explains the different asymptotic behaviour; that is, the relative energy of the keto and enol forms of acetaldehyde. It can be observed that for the water assisted system, both intermediates show the same interaction energy (5.7 kcal/mol) and thus, the reaction energy from hydrated-keto to hydrated-enol is the same (9.4 kcal/mol) as the one obtained for the isolated system. For the zeolite-catalysed system it is observed that the interaction energies of the enol and keto forms of acetaldehyde with the zeolite are significantly much larger. This could be easily understood if one considers that the zeolite is more acidic than water and its shape is more appropriate to stabilize the hydrogen-bonded intermediates. Because the zeolite interacts stronger with acetaldehyde than with hydroxyethylene, the reaction energy of the keto-enol process becomes slightly less favourable inside the zeolite (13.7 kcal mol^{-1}) than in gas phase (11.0 kcal/mol). This value increases slightly (14.4 kcal/mol) when correcting for BSSE.

The transition state for the isomerization reaction lies 8.3 kcal/mol above the HZ + keto asymptote, the energy barrier being 21.2 kcal mol^{-1} from the (Keto)HZ intermediate. As it can be observed, the catalytic effect of the zeolite is much more important than that of water. The transition state of the reaction is largely stabilized with respect to the ground state asymptote. Moreover, the energy barrier computed with respect to the keto-intermediate is much lower for the zeolite-catalysed system (21.2 kcal/mol) than for the water assisted (40.6 kcal/mol) or the gas-phase (67.9 kcal/mol) systems. This stronger catalytic effect is due to a smaller geometry reorganization of the system along the process and also to the higher acidity of the zeolite compared with water, which facilitates the proton transfer to acetaldehyde.

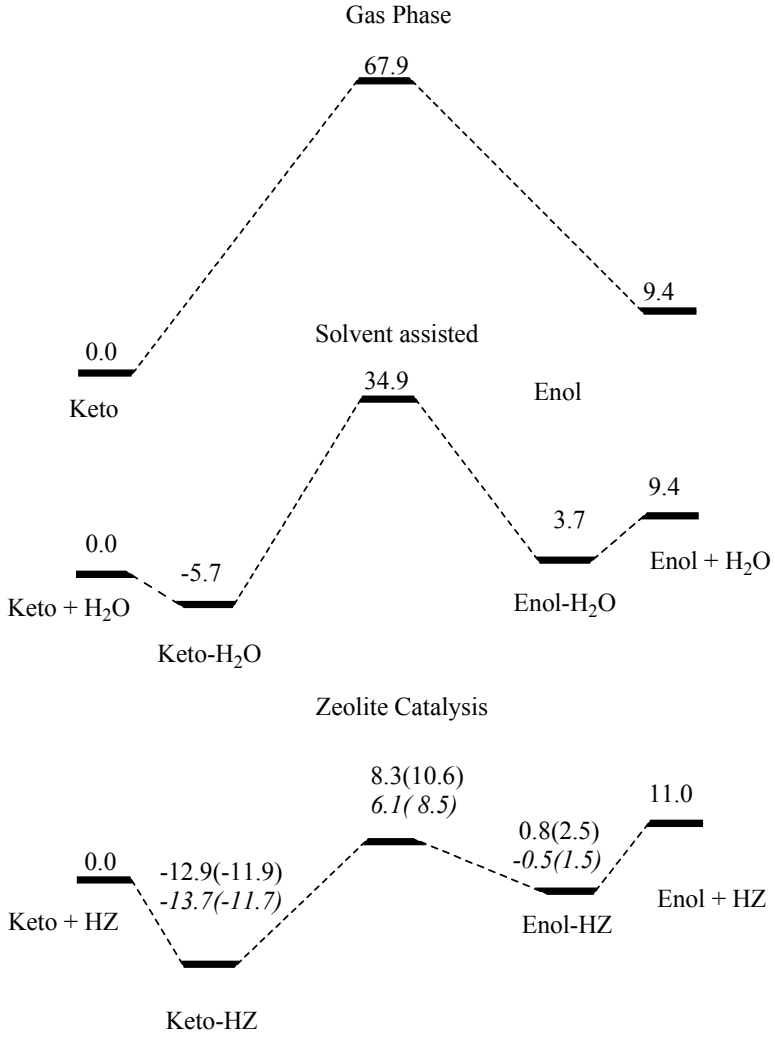

Figure 5.3 Potential energy diagram of the keto-enol isomerization of acetaldehyde in the gas phase, catalysed by a water molecule and inside HZSM-5. Relative energies with respect to the keto + catalyst asymptote (kcal/mol) plain numbers correspond to T3 results and italic ones to T5 results. In parenthesis are the counterpoise-corrected values.

The real catalytic effect can be observed from the comparison between the activation free energy in gas phase and inside the zeolite. The thermodynamic functions at 298.15 K are given in Table 5.1. The $\Delta G^{\ddagger}_{298}$ for the keto-enol isomerization inside the zeolite is 21.7 kcal mol^{-1} with respect to the HZ + Keto asymptote and 20.6 with respect to the (Keto)HZ intermediate. As expected, entropic effects destabilize the transition state structure with respect to the HZ + Keto asymptote, but the $\Delta E^{\ddagger}$ and $\Delta G^{\ddagger}_{298}$ values with respect to the (Keto)HZ intermediate are very similar, since the entropic effects are similar for both (Keto)HZ and TS structure. The $\Delta G^{\ddagger}_{298}$ value of 21.4 kcal/mol is much smaller than that corresponding to the uncatalysed (64.9 kcal/mol) or the water assisted

(44.3 kcal/mol) systems.[16] This great catalytic activity is in good agreement with the experimental results, which report easy, and fast conversions of acetaldehyde to the aldol adduct.[5,7]

Table 5.1 Relative energies (in kcal/mol) with respect to the HZ + Keto asymptote obtained with the T3 cluster. In parentheses are counterpoise corrected values.

	HZ + Keto	(Keto)HZ	TS	(Enol)HZ	HZ + Enol
ΔE	0.0	−12.9 (−11.9)	8.3 (10.6)	0.8 (2.5)	11.0
ΔH^0_{298}	0.0	−11.4 (−10.4)	6.6 (8.9)	2.7 (4.4)	11.5
ΔG^0_{298}	0.0	0.1 (1.1)	19.4 (21.7)	15.5 (17.2)	12.3

Comparing the results obtained with clusters T3 and T5, it can be observed (Figure 5.2) that the geometry parameters related to the zeolite-acetaldehyde interaction are very similar in all the stationary points. The main difference appears in the (Keto)HZ intermediate, which shows a different interaction between the methyl group of acetaldehyde and the oxygen atoms bond to aluminium. This is due to the fact that in cluster T3 these oxygen atoms are of different nature (–OH and $–OSiH_3$), the presence of terminal –OH inducing the changes in the acetaldehyde orientation. On the other hand, the results obtained with cluster T5 show that the dihedral angles defined by the Si_1, O_2, Al_3, O_4, and Si_5 atoms are far from 180^0, the value imposed in the T3 cluster calculations to avoid unreal hydrogen bond interactions. The computed values of these dihedral angles, which range from 120 to 160 degrees can, however, be the result of a lack of mechanical constraints in the zeolite. This aspect will be considered and discussed in the next section in which ONIOM2 calculations for a T3:T63 cluster will be presented. The energy profiles obtained with both T3 and T5 are very similar (see Figure 5.3). The most remarkable is that the (Enol)HZ and the TS structures are slightly more stable with the larger cluster.

5.4.2. ONIOM calculations.

Figure 5.4 presents the ONIOM optimised geometries corresponding to the stationary points of the keto-enol isomerization inside HZSM-5. For simplicity we have

only included a fragment around the active site of the global cluster and the geometrical parameters of the inner layer.

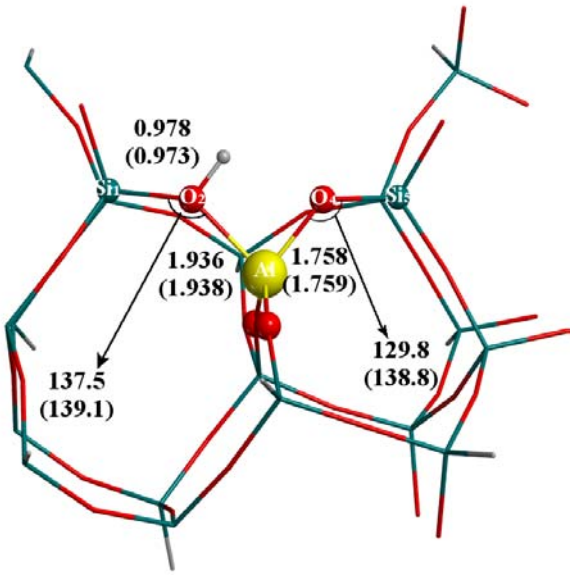

HZ

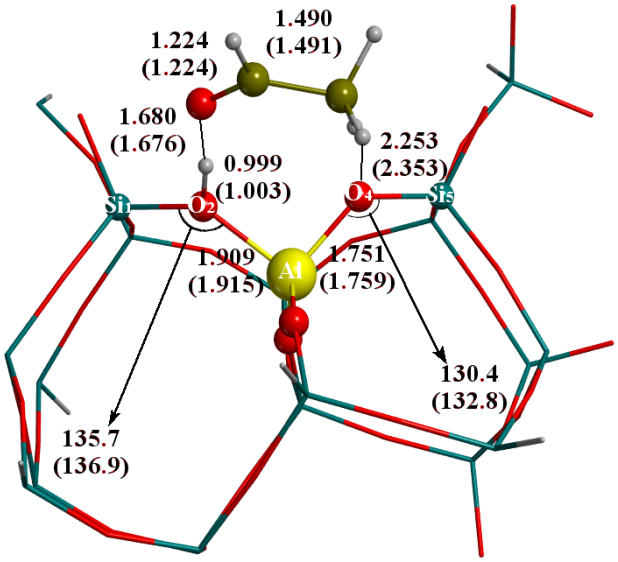

HZ(Keto)

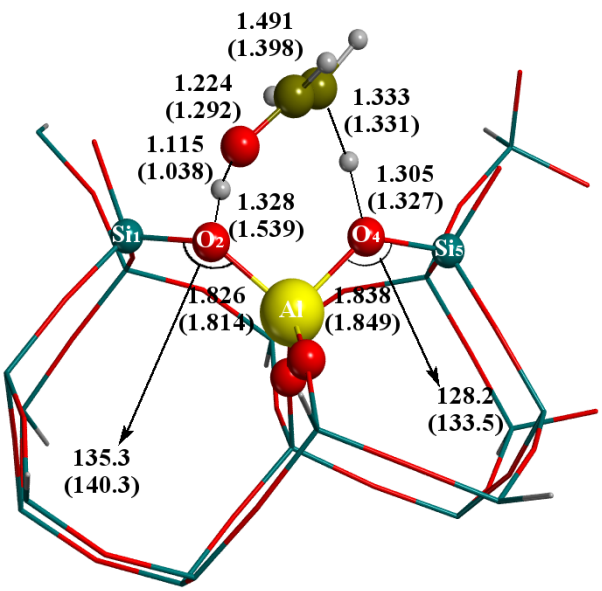

TS

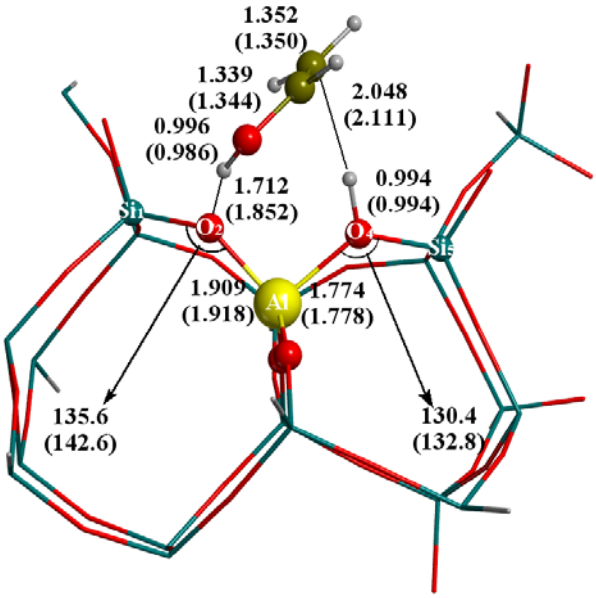

HZ(Enol)

Figure 5.4 Optimised structures of the stationary points of the keto-enol isomerization reaction obtained with T3:T63 cluster with the ONIOM2 B3LYP:MNDO (B3LYP:AM1) approaches. Distances are in Å and angles in degrees.

The comparison between the ONIOM results (Figure 5.4) and the ones obtained with the T3 and T5 clusters (Figure 5.2) shows that there are not dramatic changes on the zeolite-acetaldehyde interaction, when the cluster is increased up to 63 tetrahedra with the ONIOM procedure. Nevertheless, there are some differences on the structure of the zeolite that are worth mentioning. On one hand, it can be observed that the T3 and T5 calculations provide values of the $Al_3O_4Si_5$ angle in HZ and in the (Keto)HZ intermediate that are too large. This is due to the fact that T3 and T5 clusters are too small to take into account the constraints induced by the zeolite framework. The AlO_4Si_5 angle is not so large in the transition state or the enol adsorbed intermediate because the O_4 atom is protonated or almost protonated. On the other hand, ONIOM calculations show that the $Si_1O_2AlO_4$ and $O_2AlO_4Si_5$ dihedral angles do not change very much along the HZ(Keto)→ HZ(Enol) process, the largest variation being about $5\text{-}6^0$. However, for the T5 cluster calculations the variations of the dihedral angles are much larger. This is again due to the larger flexibility of the T5 cluster compared to the T3:T63 one considered in the ONIOM calculations.

Let us now focus on the differences between the results obtained with the different high and low level combinations. As mentioned, fully optimisations have only been done using B3LYP:MNDO and B3LYP:AM1. In contrast, B3LYP:HF energies have been obtained at the B3LYP:MNDO geometries. The choice of B3LYP:MNDO is due to the fact that Roggero et al.[40] have suggested that optimised B3LYP:MNDO structures are closer to those determined experimentally. Moreover, as it will be mentioned below both B3LYP:MNDO and B3LYP:AM1 ONIOM combinations bring to similar geometries of the active site.

Looking at the geometry parameters it is observed that, in general, the optimised geometries are quite similar with both methods. The most significant difference appears in the transition state for the O_2–H-O distance. At the B3LYP:AM1 level the proton of the zeolite is completely transferred to acetaldehyde whereas this is not the case with B3LYP:MNDO. This is probably related to the fact that the computed deprotonation energy of the zeolite at the B3LYP:AM1 level (304.5 kcal/mol) is smaller than at the B3LYP:MNDO one (327.0 kcal/mol). Considering that AM1 provides a better

description of the hydrogen bonded systems, and that the B3LYP:AM1 deprotonation energy is in much better agreement with previous QM-pot calculations[41,42] than the B3LYP:MNDO one, we expect the B3LYP:AM1 results to be more reliable. Moreover, a previous ONIOM study on the interaction of NH_3 with the hydroxyl group of the silica surface has shown that among the three semiempirical methods AM1, MNDO and PM3 used for the real system, AM1 is the one that provides better energetic results.[40]

Table 5.2 presents the energetics of the process obtained with ONIOM2 clusters. For comparison we have also included the values obtained with clusters T3 and T5. It can be observed that ONIOM2 calculations with semiempirical low levels provide smaller interaction energies between acetaldehyde and the zeolite than those obtained with the T3 and T5 clusters. This destabilization of the (Keto)HZ intermediate is more important with B3LYP:MNDO than with B3LYP:AM1. In contrast using these combinations, the (Enol)HZ intermediate becomes slightly more stable in the ONIOM calculations. As a result, the reaction energy of the (Keto)HZ → (Enol)HZ process becomes smaller. The reaction energy of 13.7 kcal/mol with T3(B3LYP) decreases to 5.9 kcal/mol with T3:T63(B3LYP:MNDO) and to 7.4 kcal/mol with T3:T63(B3LYP:AM1). This tendency was already observed when T3 was enlarged to T5. On the other hand, given that the energy of the transition state with respect to the HZ + Keto asymptote is very similar with the T3 and T63 clusters, the energy barrier of the (Keto)HZ → (Enol)HZ isomerization energy decreases somewhat when the size of the cluster is increased. In spite of that, if one considers similar entropic effects than the ones computed for T3 (see Table 5.1), the catalytic behaviour would remain more or less the same in all cases.

In contrast, comparing T3:T63(B3LYP:HF) with T3(B3LYP) results, a stabilization of the intermediates and transition state structure with respect to the HZ + Keto asymptote is observed. This stabilization affects all the structures involved in the process in a similar way and so, the global process only becomes slightly less endothermic than T3 and the energy barrier slightly decreases. Thus, in spite of the little differences in the thermodynamics, all ONIOM combinations lead to a similar energy profile with respect to (Keto)HZ intermediate. However, larger differences are observed in the relative energies of intermediates and transition state structure with respect to the reactant HZ + Keto asymptote. Comparing to the experimental adsorption energy of

acetone to HZSM-5[13], one observes that all our reported values are still smaller. Consequently, a deeper analysis is required to understand the energy differences with respect the reactant asymptote.

Table 5.2 Relative energies (kcal/mol) with respect to the HZ + Keto asymptote obtained with T3, T5 and T3:T63 clusters[a]

	HZ + Keto	(Keto)HZ	TS	(Enol)HZ	HZ + Enol
T3(B3LYP)	0.0	-12.9	+8.3	0.8	+11.0
T5(B3LYP)	0.0	-13.7	+6.1	-0.5	+11.0
T3:T63(B3LYP:MNDO)	0.0	-7.4	+8.6	-1.5	+11.0
High level	*0.0*	*-11.9*	*+5.4*	*-2.1*	
Low Level	*0.0*	*+4.5*	*+3.2*	*+0.6*	
T3:T63(B3LYP:HF)	0.0	-14.7	+1.4	-4.0	+11.0
High level	*0.0*	*-11.9*	*+5.4*	*-2.0*	
Low Level	*0.0*	*-2.8*	*-4.0*	*-2.0*	
T3:T63(B3LYP:AM1)	0.0	-9.3	+8.7	-1.9	+11.0
High Level	*0.0*	*-11.2*	*+6.0*	*-1.0*	
Low Level	*0.0*	*+1.9*	*+2.7*	*-0.9*	

[a] Relative energies corresponding to ONIOM2 calculations for cluster T3:T63 have been decomposed in two components:
HL = E_{Model}^{HL}(intermediate) – E_{Model}^{HL}(asymptote)
LL= E_{real}^{LL}(intermediate)-E_{Model}^{LL}(intermediate)-[E_{real}^{LL}(asymptote)-E_{Model}^{LL}(asymptote)]

The embedding effects introduced with ONIOM can be analysed by decomposing the global interaction energy in two terms: the High Level (HL) contribution of the model system and the low level (LL) contribution that accounts for the effects of increasing the size of the cluster. The HL term corresponds to the B3LYP energies of the inner layer but at the ONIOM optimised geometries. Comparing the HL term of the two optimised structures (B3LYP:MNDO and B3LYP:AM1) one can notice that the relative energies of the High-Level part are similar in both cases. Thus, we conclude that ONIOM (B3LYP:MNDO) and (B3LYP:AM1) produce similar constraints on the active site which leads to very similar geometries and relative energies.

The HL values are also similar to the relative energies obtained with cluster T3. This is due to the fact that the geometry and energy changes of the model system induced by the larger rigidity of the T3:T63 cluster are quite constant along the process. In spite of this, there are small differences that are worth mentioning. If one compares the absolute B3LYP energy obtained with the T3 system with that of the model system in the ONIOM2 calculation it is observed that the geometrical changes of the active site

introduced by the T3:T63 cluster are destabilizing, even though the constraints of the dihedral angles are released in the larger cluster. It is interesting to mention that, although this destabilization arises from many changes on distances and angles, part of it comes from the changes produced on the SiOAl angles and on the SiOAlO dihedral angles. As mentioned previously, the $Al_3O_4Si_5$ angle was computed to be too large in the initial asymptote and in the (Keto)HZ intermediate with T3. Because of that and all the geometry changes induced by the T3:T63 cluster, the model system in the asymptote (HZ) and in the first (Keto)HZ intermediate is destabilized 2-3 kcal/mol more than in the TS or in the second (Enol)HZ intermediate. As a result, the B3LYP relative energies of the transition state and (Enol)HZ are somewhat smaller in the ONIOM2 calculations than in the T3 ones. It is interesting to notice that these results are similar to those obtained with cluster T5.

The second term, the Low-Level one, corresponds to the energy difference between the real and the model system at the low level of calculation (AM1, MNDO or HF/3-21G). It includes (at the low level of calculation) two important factors, a destabilizing one arising from the distortion of the zeolite upon adsorption of acetaldehyde and a stabilizing one produced by the polarization of the model system by the rest of the zeolite. It can be observed in Table 5.2 that this Low-Level contribution is slightly destabilizing in all cases for MNDO and AM1 except for the (Enol)HZ intermediate at the AM1 level. Although the B3LYP:AM1 low level destabilizing contribution is smaller than for the B3LYP:MNDO one, both approaches follow the same trend along the reaction: the LL term is smaller in the product than in the reactant. This can be due to the fact that polarization of the model system by the zeolite is larger for the enol form (more polarizable) than for the keto one.

B3LYP:HF results present slightly stabilizing low-level contribution. This contribution is larger for the keto than for the enol one, the global thermodynamics (Keto)HZ → (Enol)HZ becomes slightly less endothermic (10.7 kcal/mol). An important stabilization of the transition state structure with respect the HZ + keto asymptote is observed but the energy barrier from the (Keto)HZ intermediate does not vary considerably. The relative energy difference between B3LYP:MNDO and B3LYP:HF ranges from 7.3 kcal/mol for the transition state structure to 2.1 kcal/mol for the (Enol)HZ structure

5.5 Concluding remarks

The Keto-enol isomerization of acetaldehyde inside HZSM-5 has been studied using the B3LYP density functional approach and modelling the zeolite with T3 and T5 clusters. Moreover, the effects of enlarging the cluster to T63 have been considered using the ONIOM2 approach and combining the B3LYP method with the AM1, MNDO or HF ones. It is observed that the zeolite produces an important catalytic effect on the enolization reaction. The catalytic effect is much larger than that produced by a water molecule, due to the larger acidity of the zeolite and to smaller geometry reorganisations along the process. Calculations with all clusters indicate that the adsorption of acetaldehyde to the zeolite corresponds to neutral complex and not to an ion pair.

Results with T3 and T5 are very similar. Enlarging the size of the cluster to 63 tetrahedra with the ONIOM2 approach does not affect considerably the energetic profile between intermediates and transition state structure. Results obtained with the three considered ONIOM partitions indicate that the keto-enol isomerization becomes slightly less endothermic. Larger differences are observed with respect to the adsorption energies of acetaldehyde. B3LYP:MNDO and B3LYP:AM1 leads to smaller adsorption energies compared with those obtained with T3 and T5, while single point B3LYP:HF calculations provide a somewhat larger interaction energy. However, all tested models lead to smaller adsorption energies than those reported by acetone,[13] which is supposed to present a similar adsorption energy.

The different behaviour of each combination in predicting adsorption energies, the absence of a target value, because full T63 B3LYP calculations are not possible, periodic calculations using the big HZSM-5 unit cell are too expensive and also the experimental adsorption energy has never been reported, makes not possible to conclude which methodology is the most accurate. Moreover, the significant differences with the experimental value reported for acetone suggest that more analysis is needed to verify the reliability of different ONIOM approaches for determining adsorption energies. Because of that, we decided to study a different system for which experimental data is available and periodic calculations could be performed. This study is the adsorption of NH_3 on Chabazite, which will be presented in the next chapter.

References

(1) Carey, F. A.; Sundberg, R. Reactions of Carbon Nucleophiles with Carbonyl Groups. In *Advanced Organic Chemistry*; Plenum Press: New York, 1983; Vol. B; pp 43.

(2) Hölderich, W.; Hesse, M.; Näumann, F. *Angew. Chem. Int. Ed. Engl.* **1988**, *27*, 226.

(3) Kubelková, L.; Nováková, J. *Zeolites* **1991**, *11*, 822.

(4) Corma, A. *Chem. Rev.* **1995**, *95*, 559.

(5) Chavez Diaz, C. D.; Locatelli, S.; Gonzo, E. E. *Zeolites* **1992**, *12*, 851.

(6) Xu, T.; Munson, E. J.; Haw, J. F. *J. Am. Chem. Soc.* **1994**, *116*, 1962.

(7) Biaglow, A. I.; Gorte, R. J.; White, D. *J. Phys. Chem.* **1993**, *97*, 7135.

(8) Dumitriu, E.; Hulea, V.; Fechete, I.; Auroux, A.; Lacaze, J.-F.; Guimon, C. *Micropor. and Mesopor. Mater.* **2001**, *43*, 341.

(9) Gorte, R. J.; White, D. *Top. Catal.* **1997**, *4*, 57.

(10) Hagen, G. P. US Pat 4,433,174 (Standard Oil Co (Indiana)) February 21 1984

(11) Höelderich, W.; Hupfer, L.; Schneider, K. US Pat 4,866,210 (BASF Aktiengesellschaft (Ludwigshafen)) September 12, 1989

(12) Florián, J.; Kubelková, L. *J. Phys. Chem.* **1994**, *98*, 8734.

(13) Šepa, J.; Lee, C.; Gorte, R. J.; White, D.; Kassab, E.; Evleth, E. M.; Jessri, H.; Allavena, M. *J. Phys. Chem.* **1996**, *100*, 18515.

(14) Kassab, E.; Seiti, K.; Allavena, M. *J. Phys. Chem.* **1991**, *95*, 9425.

(15) Coitiño, E. L.; Tomasi, J.; Ventura, O. N. *J. Chem. Soc. Faraday Trans.* **1994**, *90*, 1745.

(16) Rodríguez-Santiago, L.; Vendrell, O.; Tejero, I.; Sodupe, M.; Bertran, J. *Chem. Phys. Lett.* **2001**, *334*, 112.

(17) Vreven, T.; Morokuma, K. *J. Comput. Chem.* **2000**, *21*, 1419.

(18) Svensson, M.; Humbel, S.; Froese, R. D. J.; Matsubara, T.; Sieber, S.; Morokuma, K. *J. Phys. Chem.* **1996**, *100*, 19357.

(19) Maseras, F.; Morokuma, K. *J. Comput. Chem.* **1995**, *16*, 1170.

(20) Eichler, U.; Kölmel, C. M.; Sauer, J. *J. Comput. Chem.* **1996**, *18*, 463.

(21) Sierka, M.; Sauer, J. *J. Chem. Phys.* **2000**, *112*, 6983.

(22) Rodríguez-Santiago, L.; Sierka, M.; Branchadell, V.; Sodupe, M.; Sauer, J. *J. Am. Chem. Soc.* **1998**, *120*, 1545.

(23) Becke, A. D. *J. Chem. Phys.* **1993**, *98*, 5648.

(24) Lee, C.; Yang, W.; Parr, R. G. *Phys. Rev. B* **1988**, *37*, 785.

(25) Hehre, W. J.; Ditchfield, R.; Pople, J. A. *J. Chem. Phys.* **1972**, *56*, 2257.

(26) Krishnan, R.; Binkley, J. S.; Seeger, R.; Pople, J. A. *J. Chem. Phys.* **1980**, *72*, 650.

(27) McLean, A. D.; Chandler, G. S. *J. Chem. Phys.* **1980**, *72*, 5639.

(28) Boys, S. F.; Bernardi, F. *Mol. Phys.* **1970**, *19*, 553.

(29) Dewar, M. J. S.; Zoebisch, E. G.; Healy, E. F.; Stewart, J. J. P. *J. Am. Chem. Soc.* **1985**, *107*, 3902.

(30) Dewar, M. J. S.; Thiel, W. *J. Am. Chem. Soc.* **1977**, *99*, 4899.

(31) Hartree, D. R. *Proc. Cambridge Phil. Soc.* **1928**, *24*, 89.

(32) Fock, V. *Z. Physik* **1930**, *61*, 126.

(33) Rappé, A. K.; Casewit, C. J.; Colwell, K. S.; Goddard III, W. A.; Skiff, W. M. *J. Am. Chem. Soc.* **1992**, *114*, 10024.

(34) Frisch, M. J.; Trucks, G. W.; Schlegel, H. B.; Scuseria, G. E.; Robb, M. A.; Cheeseman, J. R.; Zakrzewski, V. G.; Montgomery, J. A.; Stratmann, R. E.; Burant, J. C.; Dapprich, S.; Millam, J. M.; Daniels, A. D.; Kudin, K. N.; Strain, M. C.; Farkas, O.; Tomasi, J.; Barone, V.; Cossi, M.; Cammi, R.; Mennucci, B.; Pomelli, C.; Adamo, C.; Clifford, S.; Ochterski, J.; Petersson, G. A.; Ayala, P. Y.; Cui, Q.; Morokuma, K.; Malick, D. K.; Rabuck, A. D.; Raghavachari, K.; Foresman, J. B.; Cioslowski, J.; Ortiz, J. V.; Baboul, A. G.; Stefanov, B. B.; Liu, G.; Liashenko, A.; Piskorz, P.; Komaromi, I.; Gomperts, R.; Martin, R. L.; Fox, D. J.; Keith, T.; Al-Laham, M. A.; Peng, C. Y.; Nanayakkara, A.; Gonzalez, C.; Challacombe, M.; Gill, P. M. W.; Johnson, B. G.; Chen, W.; Wong, M. W.; Andres, J. L.; Head-Gordon, M.; Replogle, E. S.; Pople, J. A. Gaussian 98; Gaussian Inc.: Pittsburgh, 1998.

(35) Pazé, C.; Bordiga, S.; Lamberti, C.; Salvalaggio, M.; Zecchina, A.; Bellussi, G. *J. Phys. Chem. B* **1997**, *101*, 4740.

(36) Scott, A. P.; Radom, L. *J. Phys. Chem.* **1996**, *100*, 16502.

(37) Brändle, M.; Sauer, J.; Dovesi, R.; Harrison, N. M. *J. Chem. Phys.* **1998**, *109*, 10379.

(38) Brändle, M.; Sauer, J. *J. Mol. Catal. A: Chemical* **1997**, *119*, 19.

(39) Paukshtis, E. A.; Malysheva, L. V.; Stepanov, V. G. *React. Kinet. Catal. Lett.* **1998**, *65*, 145.

(40) Roggero, I.; Civalleri, B.; Ugliengo, P. *Chem. Phys. Lett.* **2001**, *341*, 625.

(41) Eichler, U.; Brändle, M.; Sauer, J. *J. Phys. Chem. B* **1997**, *101*, 10035.

(42) Sierka, M.; Eichler, U.; Datka, J.; Sauer, J. *J. Phys. Chem. B* **1998**, *102*, 6397.

6. NH_3 adsorption on HCHA

6.1 Introduction

The Brønsted acid sites in zeolites cannot be characterized by X-Ray diffraction, since they do not present any periodicity.[1] Thus, normally zeolite acidity is analysed from indirect measurements, such as the study of the interaction of basic probe molecules with H^+ exchanged zeolites.[2,3]

Several techniques as well as different probe molecules have been used to characterize the acidic activity of zeolites.[2] Mainly, the IR[4-10] and NMR[5,11] spectroscopies and temperature programmed desorption[8-10,12,13] and microcalorimetry[14-16] experiments have been used for this purpose. Among the large variety of probe molecules employed, ammonia has been one of the most widely used. It must be pointed out that, nowadays, there is a large agreement in the fact that only one experimental technique and only one probe molecule cannot provide a complete comprehension of the Brønsted acidity of a zeolite framework. Multi-technique studies with different zeolite frameworks, Si/Al ratios as well as several probe molecules are needed.[2,6]

IR spectroscopy is mainly used to analyse the nature of the interaction of small molecules with Brønsted acid sites.[2] Great efforts have been done to identify if the interaction between the zeolite and the probe molecule occurs through a neutral hydrogen bond or through an ion pair; that is, if the probe molecule is able to deprotonate the zeolite. Temperature programmed desorption (TPD) experiments consist on determining the number of molecules desorbed at each temperature during a progressive increase of the temperature.[2] They are used to identify the number and different types of interactions when a probe molecule is introduced in the zeolite framework. Moreover, these experiments are also used to evaluate the number of acid sites. Microcalorimetry experiments are used to determine the interaction energy between the probe molecule and the zeolite at different coverages.[2,15] When they are performed at high temperatures (around 400K) weak interactions are avoided and one can observe only those interactions related with strong acid sites. At these conditions, interaction energies extrapolated to 0 coverage are normally assigned to the strongest acid site while coverage in the region of one probe molecule per aluminium are associated to Brønsted acidity.[15]

The interaction of ammonia with acidic zeolites has been largely reported.[2,3,5,8-10,12-16] It is well established that ammonia is basic enough to deprotonate the acidic

zeolite to form an ion-pair (IP); that is, NH_4^+-Z^-.[5,8,10] This is observed in the IR spectra mainly by the large decrease of the band at ~3600 cm^{-1}, associated with the Brønsted site, and the formation of a characteristic band at 1680 cm^{-1} accompanied with other bands in the 1400-1500 cm^{-1} range associated to the NH_4^+ cation. [5,8,10] The binding energy is in the range 33-38 kcal/mol for poor aluminium H-ZSM-5 and H-MOR,[2,13,14,16] while for H-Y the interaction energy is 26.3 kcal/mol.[14]

Although the experimental adsorption energy of NH_3 on Chabazite is not available in the literature, the above reported values suggest that the adsorption energy may be close to that of zeolites with 10 or 8-membered rings. That is, we expect that the adsorption energy of ammonia in Chabazite to be in the 33-38 kcal/mol range.

The first theoretical studies analysing the adsorption of probe molecules with Brønsted acid sites appeared in the beginning of last decade. Ammonia has also been largely chosen in theoretical studies as probe molecule interacting with the Brønsted site of the zeolite.[17-28] Two aspects are generally considered: the comparison with experimental results and the difficulty to reproduce the relative stability of neutral NH_3 hydrogen bonded form (HB) and ion pair (NH_4^+) structure (IP).

The first studies used small zeolite clusters as a model of the real system and they performed MP2 single point calculations over HF optimised geometries.[19-21] Depending on the basis set and the number of hydrogen bonds formed between NH_3 or NH_4^+ and the zeolite, the relative stability between the hydrogen bonded form NH_3-HZ and ion pair NH_4^+-Z^- varied, indicating that the methodology used led to very similar interaction energies for both structures. These results do not agree with experiments, in which only the NH_4^+-Z^- form is observed.

To improve the model, embedded clusters were considered.[17,22-26] Teunissen et al. included an embedding correction potential which accounts for long-range effects.[17,22] With this scheme and using MP2 single point calculations at HF geometries they observed that the ion pair form (NH_4^+-Z^-) becomes around 12 kcal/mol more stable than the hydrogen bonded one. These results are similar to those obtained from periodic HF calculations.[17] Similar conclusions were obtained by Brändle et al.[25] using the QM-Pot scheme,[29,30] in which the embedding is introduced by a force field with periodic conditions (see chapter 2). They also used HF as a quantum level and for Chabazite, they

found that the energy difference between the ion pair and the hydrogen-bonded structure is about 9 kcal/mol.

More recently, the use of DFT as quantum level has been adopted.[23,24,26,28] Brändle et al.[26] have studied the NH_3 interaction with several zeolite frameworks and they have observed that the ion pair structure is more stable than the hydrogen bonded complex by 5-7 kcal/mol.[26] Kyrlidis et al.[23] and Vollmer et al.[24] have reported similar results using DFT and point charges as embedding scheme.

Nowadays, the inclusion of long range effects seems to be very important to reproduce the interaction energies between probe molecules and acidic zeolites, especially when an ion pair structure is formed. Several approaches have been developed and used to model these effects. However, the nature and magnitude of these long-range effects are still unclear. Moreover, most of these approaches have still not been used in reactivity studies as they do not include efficient strategies to localize transition state structures. On the other hand, ONIOM approach[31-33] is increasingly being used to study big systems[34,35] and its potentiality in modelling solids has been suggested.[36,37] The ONIOM approach is interesting since it is a cost-efficient method and also it can be useful to study reactivity inside zeolites. However, before the beginning of this thesis no study using the ONIOM approach to model zeolites and related materials had appeared and only very few have been published during this period.[36-42]

6.2 Goal

The aim of the present study is to analyse the accuracy of several approaches (free and ONIOM clusters and periodic calculations) in reproducing the NH_3 adsorption on acidic Chabazite. Special efforts have been focused on determining a good strategy to use ONIOM approach in the modelling of acidic zeolites. For this purpose several level combinations as well as different partitions of the inner and outer layers have been considered. Moreover, the analysis of the long-range effects is accomplished by comparing the adsorption energies obtained with free and ONIOM clusters with periodic calculations.

6.3 Computational details

Three different models of the zeolite have been considered and they are presented in Figure 6.1: a) The T5 cluster, which only includes the local effects around the Brønsted site, b) Periodic calculations using a local expansion of atomic orbitals and c) The hybrid ONIOM approach for a 48 tetrahedra cluster constructed by 4 unit cells, in which the inner layer has 12 tetrahedral (T12) formed by the inclusion of the 8-membered ring and the two four-membered ring around the active site. This cluster will be called hereafter T12:T48. Both for periodic and ONIOM cluster calculations the Si/Al ratio is maintained to 11.

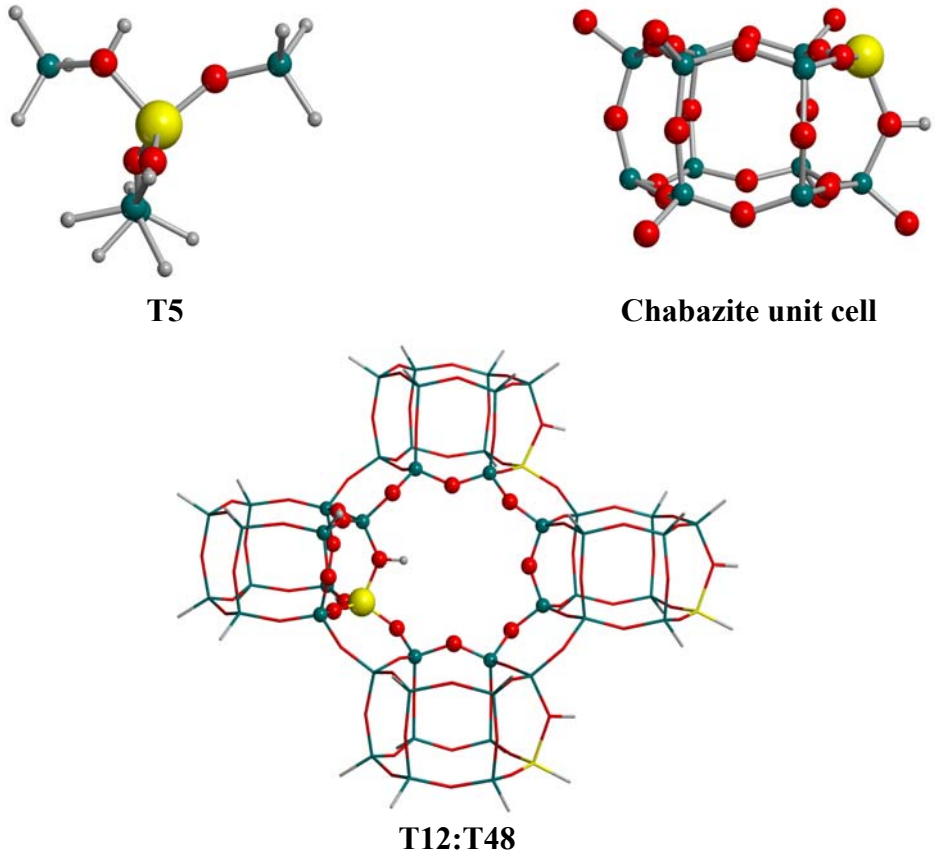

Figure 6.1 Zeolite models used in the NH_3 adsorption on Chabazite. Stick atoms are computed at the lower level of theory.

Both HF[43,44] and B3LYP[45,46] levels of theory have been used. Two different basis set have been employed: 1) a double-ζ plus polarization quality basis set adapted to be used in periodic calculations.[47] For Si, Al, O and H this basis set is equal to that named

BS1 in chapter 4 and hereafter will be called BSA. 2) The Pople 6-31++G(d,p)[48] basis set (BSB). In ONIOM approach the employed low levels of theory are MNDO[49], AM1[50] and HF/3-21G. Basis set superposition error has been corrected using the counterpoise procedure.[51] The considered fragments are NH_4^+ and Z^- as, although they do not correspond to the reference asymptote, they are the fragments that one can chemically distinguish in the adsorbed complex. In ONIOM calculations BSSE has only been estimated for the inner layer.

Periodic calculations have been performed using the CRYSTAL package[52] while cluster ones have been performed using the GAUSSIAN98 package[53].

Periodic calculations have been done during two short stays in the University of Torino in collaboration with Prof. Piero Ugliengo.

6.4 Results and discussion

6.4.1 T5 cluster modelling

Figure 6.2 shows the B3LYP/BSA (HF/BSA) optimised structures of HZ, NH_3-HZ and NH_4^+-Z^- systems. Adsorption energies with the two BSA and BSB basis sets are given in Table 6.1. Geometry parameters obtained with BSB (HF and B3LYP) are very similar to those obtained with BSA, the computed differences being always smaller than 0.05 Å, except for the longest NH-O_4 distance in the NH_3-HZ structure (see below) for which BSB basis set leads to considerably longer distances (2.20 Å and 3.41 Å at B3LYP and HF respectively). At the HF level of theory only the hydrogen bonded minimum (HB) is found, while at the B3LYP level of theory two different minima on the potential energy surface are located: the HB and the ion pair (IP) structures. At the B3LYP level, the HB structure presents two hydrogen bonds one between the proton of the Brønsted site and the N of ammonia and the other one between a proton of NH_3 and an oxygen of the zeolite. The first one presents a shorter $O_2H\cdots N$ distance suggesting that it is stronger. The IP structure presents two strong hydrogen bonds between the protons of ammonium and the oxygen atoms bonded to the central aluminium. These hydrogen bonds produce

an important geometry distortion of both fragments. The adsorption energy at the HF level ranges between –14.6 and –17.2 kcal/mol. On the other hand the energy obtained at the B3LYP level is about 4.5-7 kcal/mol higher than at the HF one. Both IP and HB structures present very similar adsorption energies. When a larger basis set is used (BSB), considerably smaller adsorption energies are obtained. The adsorption energies obtained with both basis sets become closer after including counterpoise correction.

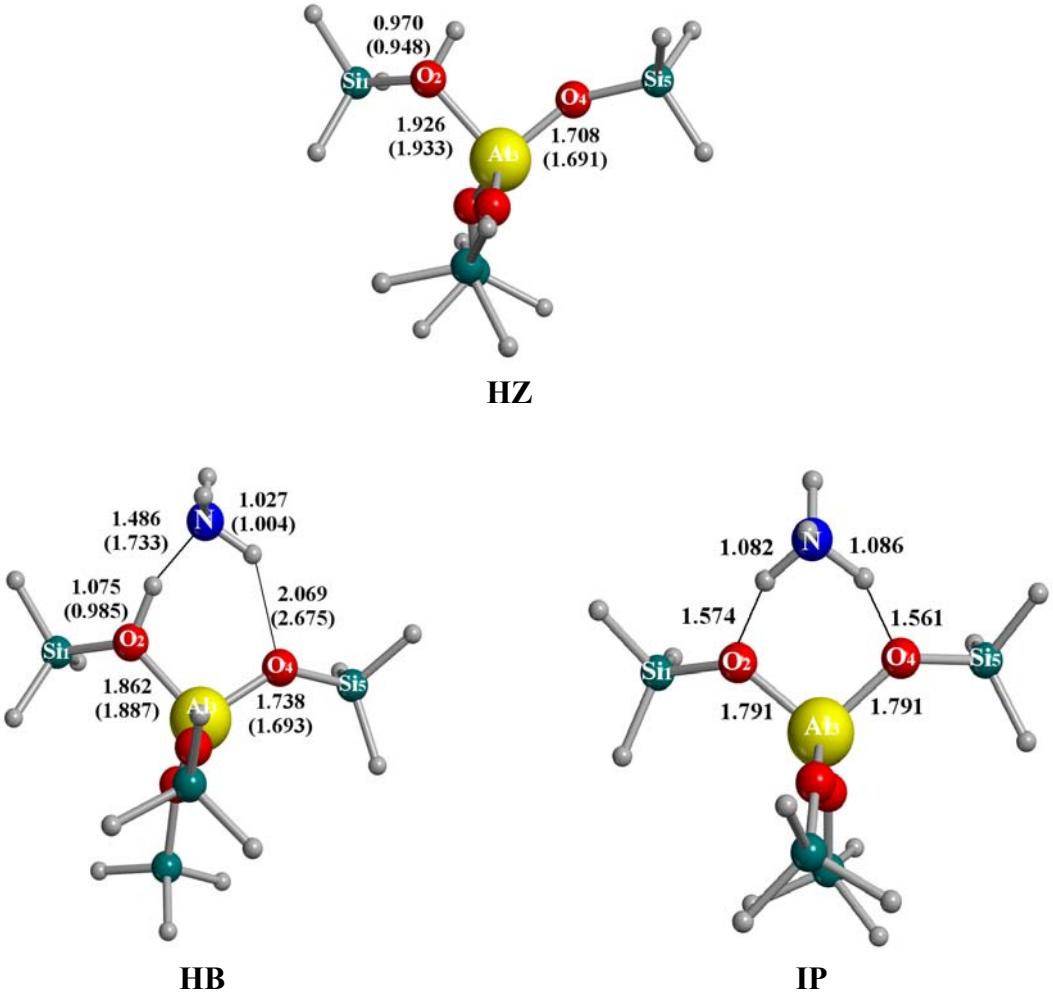

Figure 6.2 T5 optimised structures of HZ, HB and IP species, using B3LYP/BSA (HF/BSA) level of theory. Distances in Å.

Table 6.1 Adsorption energies (in kcal/mol) of NH_3 on HCHA, using T5 cluster model. In parenthesis BSSE corrected values

	HF		B3LYP	
Struct.	BSA	BSB	BSA	BSB
HB	−17.2	−14.6	−24.0	−19.0
IP			−24.2 (1−9.6)	−19.5 (−17.6)

When comparing the T5 results with the available experimental data, several discrepancies appear. First of all, IR experiments suggest that the interaction between H^+ exchanged zeolites and NH_3 is through an ion pair structure,[5,8,10] whereas with the T5 cluster both IP and HB structures are localized and predicted to have similar stabilities. Moreover, the interaction energy obtained from microcalorimetry experiments ranges between -33 kcal/mol and -38 kcal/mol,[13,15,16] which are notably higher than the value obtained with T5 B3LYP/BSB calculations (-17.6 kcal/mol).

Concluding, T5 cluster does not provide a correct description of NH_3 adsorption in H^+ exchanged zeolites. These results are in contrast with those obtained in the keto-enol isomerization of acetaldehyde where T5 predicts correctly the hydrogen-bonded structure of acetaldehyde (chapter 5).

6.4.2 Periodic calculations

Figure 6.3 presents a fragment of the optimised Chabazite and adsorbed complex. Adsorption energy at the HF/BSA and B3LYP/BSA levels of theory are also included. In both cases the adsorption of NH_3 takes place through an ion pair structure in which the ammonium ion lies in the 8-membered ring plane forming three hydrogen bonds with oxygens of the ring. It must be pointed out that only one of these bonds involves an oxygen atom bonded to aluminium (O_5), while the other two occur with O_1 and O_9 respectively. The three hydrogen bonds present different distances, the shorter one corresponding to that established with O_5. The other two NH-O distances are larger than 1.9 Å and the N-H-O angles deviate significantly from 180º. Consequently, geometry parameters suggest that one of the hydrogen bonds is much stronger than the other two. This is in contrast with the results obtained for T5, where both hydrogen bonds are strong. Oxygen atoms bonded to aluminium are more basic than those bonded to Si. So, the Al-O···H hydrogen bonds are expected to be stronger than the Si-O···H ones.

However, the formation of two hydrogen bonds involving two oxygen atoms bonded to the same Al requires an important geometry reorganization. The obtained results are the consequence of the balance between both effects.

The computed B3LYP interaction energy (–36.9 kcal/mol) is much larger than that obtained with the T5 cluster (–24.2 kcal/mol). Assuming a similar basis set superposition error, the corrected adsorption energy from periodic calculations would be about –32 kcal/mol, in good agreement with the experimental data available for other H^+ exchanged zeolites. Thus, periodic B3LYP is a good strategy to model these system and could be chosen as target value. On the contrary, as geometry parameters suggest, HF underestimates the adsorption energy by around 25%.

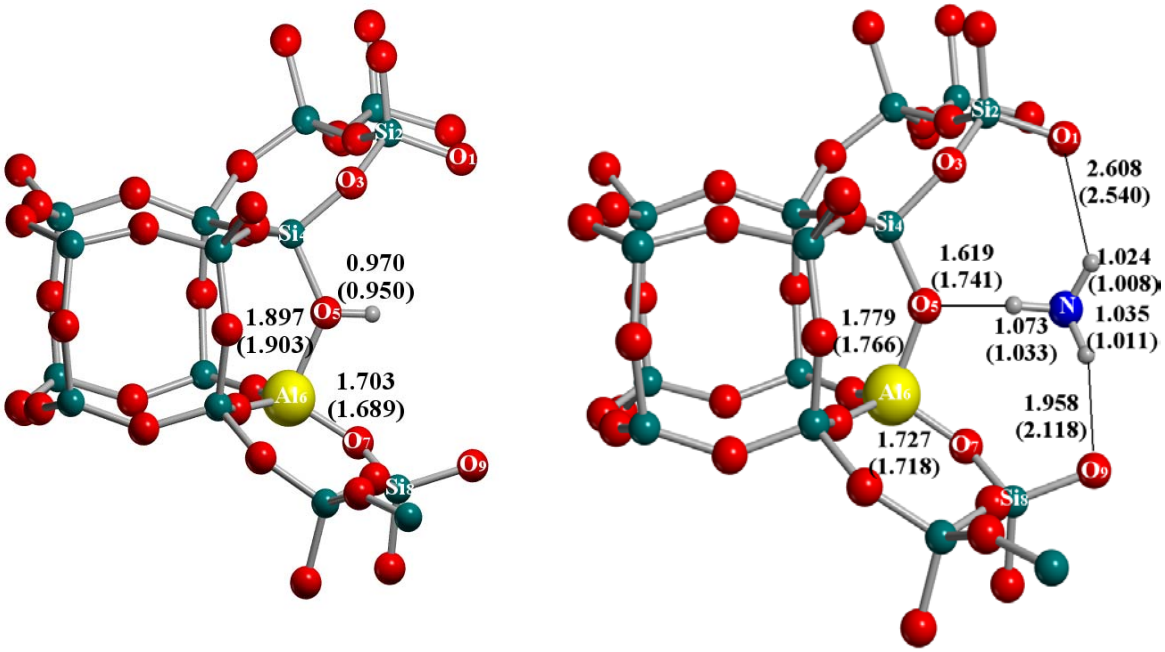

HCHA **IP**

-36.9 (27.8) kcal/mol

Figure 6.3 Optimised HCHA and IP structures and adsorption energies obtained with periodic B3LYP (HF) calculations. Distances in Å

HF results are similar to those reported by Brändle et al.[25] on the NH_3 adsorption on HCHA using the QM-Pot scheme and HF periodic calculations with a larger basis set. Their optimised QM-Pot structures present three hydrogen bonds, only one of them involving an oxygen atom bonded to aluminium. Moreover, single point periodic

calculations at the optimised QM-Pot geometry led to an adsorption energy of –23.9 kcal/mol. The agreement is also observed with Teunissen et al. periodic calculations.[17]

Up to now we have shown the good performance of periodic DFT calculations on modelling acidic zeolites. However, periodic calculations are expensive and at present accurate periodic calculations are not feasible for zeolites with big unit cells. For example, the computation of the widely used H-ZSM-5, which has a unit cell with 96 tetrahedra (288 atoms), is not possible. Thus, we have studied the performance of a less computationally demanding scheme such as ONIOM. Since the HF level of theory is not accurate enough to reproduce the experimental value only B3LYP will be used as high level.

6.4.3 ONIOM clusters.

Figure 6.4 presents a fragment of the optimised HZ and NH_4^+-Z^- (IP) structures obtained with ONIOM combinations. Table 6.2 shows the ONIOM NH_3 adsorption energies. For comparison, the T5 and periodic results are also included. The total adsorption energy is divided in high and low level contributions. The first one corresponds to the adsorption energy considering only the inner layer computed at the high level of theory, while the second term indicates the correction produced when one enlarges the cluster.

The interaction of ammonia with HCHA takes place through the NH_4^+-Z^- ion pair. The possible formation of a HB structure, NH_3-HZ, has been explored at the B3LYP/BSA:MNDO level. However, all trials evolved to the ion pair structure. As in the periodic calculations NH_4^+ lies in the 8-membered ring with three of its protons pointing to three oxygen atoms of the ring. Again, only one of these three oxygen atoms is bonded to aluminium, the O_5···H distance being the shortest one. The other two O···H distances are always longer than 2Å, so that the hydrogen bonding interaction is weaker. This disposition of the NH_4^+ is very similar to that observed in periodic calculations, which cannot be represented using T5 as a model for the zeolite. Consequently, by enlarging T5 cluster, which is not able to model the adsorption of ammonia in Chabazite, up to ONIOM T12:T48 cluster one can reproduce the formation of the ion pair structure and the coordination mode obtained in periodic calculations and suggested by experiments.

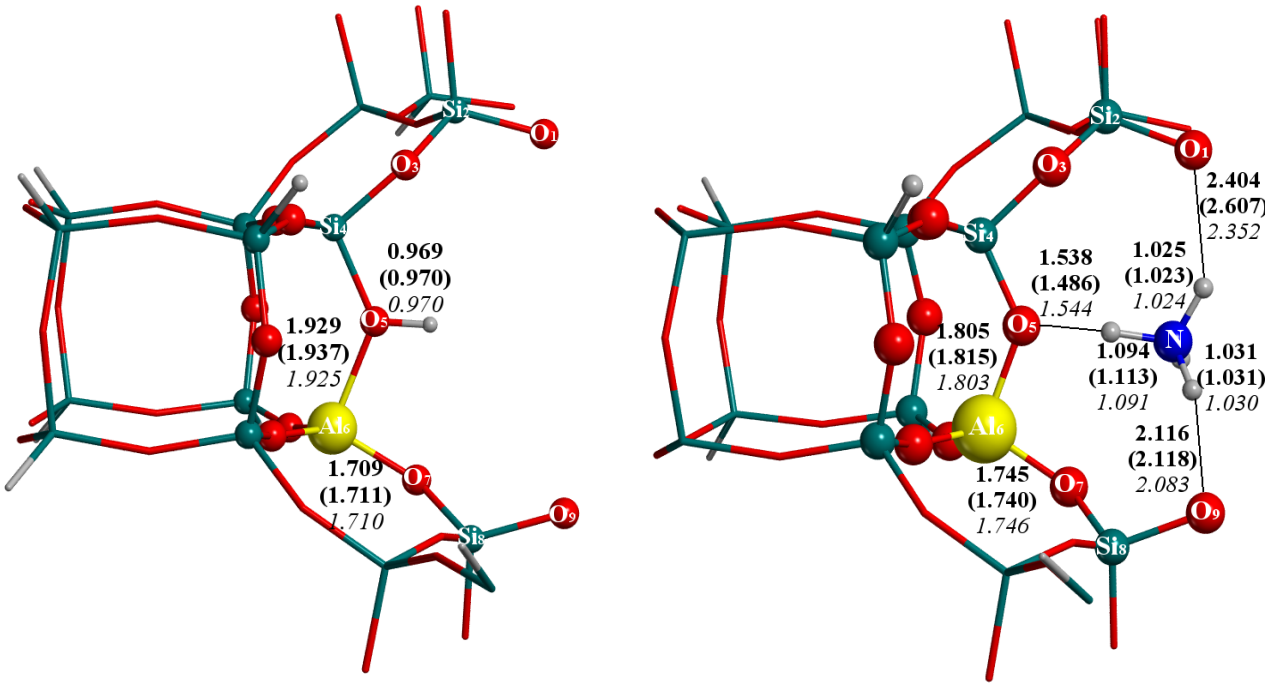

HZ IP

Figure 6.4 Optimised HZ and IP structures obtained with ONIOM approach and BSA. Bold values corresponds to B3LYP:MNDO level combination, in parenthesis B3LYP:AM1 ones and in Italic those obtained with B3LYP:HF. Distances are in Å

Table 6.2 Relative energies (in kcal/mol) with respect to the HZ + NH_3 asymptote obtained at B3LYP/BSA level and using T5, T12:T48[a] and periodic calculations.

Model	Low-Level	ΔE^b	*HL*	*LL*
T5		–24.2 (–19.6)		
T12:T48	MNDO	–32.5 (–27.5)	–32.1	–0.4
	AM1	–28.9 (–24.1)	–31.2	+2.3
	HF/3-31G	–34.8 (–29.9)	–32.1	–2.7
	HF/3-21G//MNDO	–35.0 (–30.0)	–32.1	–2.9
Periodic		–36.9		

[a] Adsorption energies have been decomposed in two components:
$HL = E_C^{HL}(NH_4^+\text{-}Z^-) - E_C^{HL}(NH_3\text{+}HZ)$
$LL = E_{real}^{LL}(NH_4^+\text{-}Z^-) - E_C^{LL}(NH_4^+\text{-}Z^-) - [E_{real}^{LL}(NH_3\text{+}HZ) - E_C^{LL}(NH_3\text{+}HZ)]$
[b] In parenthesis BSSE corrected values

Comparing the geometry parameters obtained with the different ONIOM partitions it is observed that all three low level methods lead to similar geometries around the Brønsted site. The shortest hydrogen bond varies less than 0.05 Å, while the largest differences are observed for the longer ones. Finally, the comparison with periodic calculations reveals that the geometry around the Brønsted acid site obtained with ONIOM clusters is quite close to that obtained with periodic calculations.

The NH_3 adsorption energy ranges from –28.9 to –34.8 kcal/mol. These values are closer to those computed with periodic B3LYP (–36.9 kcal/mol) than those obtained with T5 (–24.2 kcal/mol) indicating that our ONIOM cluster appears to be accurate enough for modelling the NH_4^+-CHA^- interaction. However, the adsorption energy is highly dependent on the low level used. Semiempirical methods bring to weaker NH_4^+-CHA^- interactions than those obtained with the B3LYP:HF ONIOM combination. Moreover, B3LYP:HF adsorption energy (–34.8 kcal/mol) is very close to that computed with periodic B3LYP (–36.9 kcal/mol). Correcting for basis set superposition error decreases the adsorption energy by 5 kcal/mol.

Analysing the high and low level contributions to the adsorption energy, it is clearly observed that the gain in binding energy when going from T5 to T12:T48 is mainly due to the high level contribution which arises from the fact that now we are considering the whole 8-membered ring. The contribution of the low level is always small. Thus, the inclusion of more oxygens, which allows the formation of less distorted hydrogen bonds and of the 8-membered ring is of great importance to describe accurately the adsorption of NH_3 in HCHA. It must be pointed out that high-level contributions are very similar within all ONIOM2 combinations (the largest difference is 0.8 kcal/mol) indicating that the reported little geometry differences do not affect the adsorption energy and that all low-levels used introduce similar geometry constraints due to the zeolite framework. The differences in the adsorption energy between all the used combinations arise from the low level contribution, as in the previous study of acetaldehyde (Chapter 5). AM1 contribution slightly destabilizes the NH_4^+-CHA^- interaction, MNDO one slightly increase the adsorption energy and finally the HF/3-21G contribution is higher and favours the NH_4^+-CHA^- formation. These results suggest that the nature of the interaction can be described with any of the ONIOM combinations. However, although

the low level contribution is not the most important part of the interaction energy, HF/3-21G is needed to approach the experimental adsorption energy.

One of the factors that can influence the adsorption energy of NH_3 on Chabazite is the deprotonation energy of HZ. Thus, we have computed the deprotonation energy considering the three ONIOM combination and the obtained values are reported in Table 6.3. All obtained values agree with the previously reported range for zeolites (280-330 kcal/mol)[2,4,28,54-56] indicating the reliability of ONIOM clusters to compute this property.

Table 6.3 Deprotonation energy[a] of HZ (in kcal/mol) using B3LYP/BSA as high level.

Low-level	ΔE	HL	LL
MNDO	315	*302*	*13*
AM1	305	*302*	*3*
HF/3-21G	296	*301*	*–6*

[a] Deprotonation energies have been decomposed in two components:
$HL = E_C^{HL}(Z^- + H^+) - E_C^{HL}(HZ)$
$LL = E_{real}^{LL}(Z^- + H^+) - E_C^{LL}(Z^- + H^+) - [E_{real}^{LL}(HZ) - E_C^{LL}(HZ)]$

The computed value using B3LYP/BSA:HF/3-21G is lower than that computed with the other two ONIOM combinations. This smaller proton affinity arises mainly from the low-level contribution, since high level contributions are almost identical. Although this lower deprotonation energy suggests a weaker interaction with NH_4^+, present results indicate that the interaction is stronger with B3LYP:HF/3-21G. Thus other factors must be involve.

It must be pointed out that ONIOM2(B3LYP/BSA:HF/3-21G) optimisations are very expensive and thus, the use of this ONIOM combination does not represent an important computational gain with respect to the periodic calculation. Considering that all low levels lead to similar geometry constraints, we tested the reliability of single point B3LYP:HF calculations at the B3LYP:MNDO geometries. The obtained results (Table 6.2) are very similar to those obtained at the B3LYP:HF optimised geometries, while the computational cost is much lower.

The differences observed between T5 and T12:T48 indicate that the inclusion of the whole channel is of great importance to reproduce accurately the adsorption of NH_3 on acidic Chabazite. The inclusion of the channel stabilizes mainly the ion pair form,

which becomes the only energy minimum and changes the coordination mode of the formed NH_4^+. In addition to this, the comparison between ONIOM clusters and full periodic calculations indicates that the long-range effects are small and thus a good description of the system could be obtained with the cluster approach. However, this cluster should include the whole ring and also the appropriate zeolite framework to obtain a realistic constraint of the ring. Thus, the use of ONIOM clusters seems a good strategy for acidic zeolites.

The employed basis set is quite small. In order to analyse the basis set size effect we performed ONIOM calculations using as high level B3LYP/BSB and the previous used low-levels (MNDO, AM1 and HF). Figure 6.5 shows the near environment of the Brønsted acid site optimized structures and Table 6.4 summarizes the adsorption energies obtained with the larger basis set. The effect of increasing the basis set does not produce important geometry differences (Figures 6.4 and 6.5) but the adsorption energy decreases considerably. This decrease comes mainly from the High-level contribution. However, when the energy is corrected for BSSE the obtained results are very similar. This indicates that, although the small BSA leads to too high interaction energies, they are reasonably corrected when counterpoise correction is added.

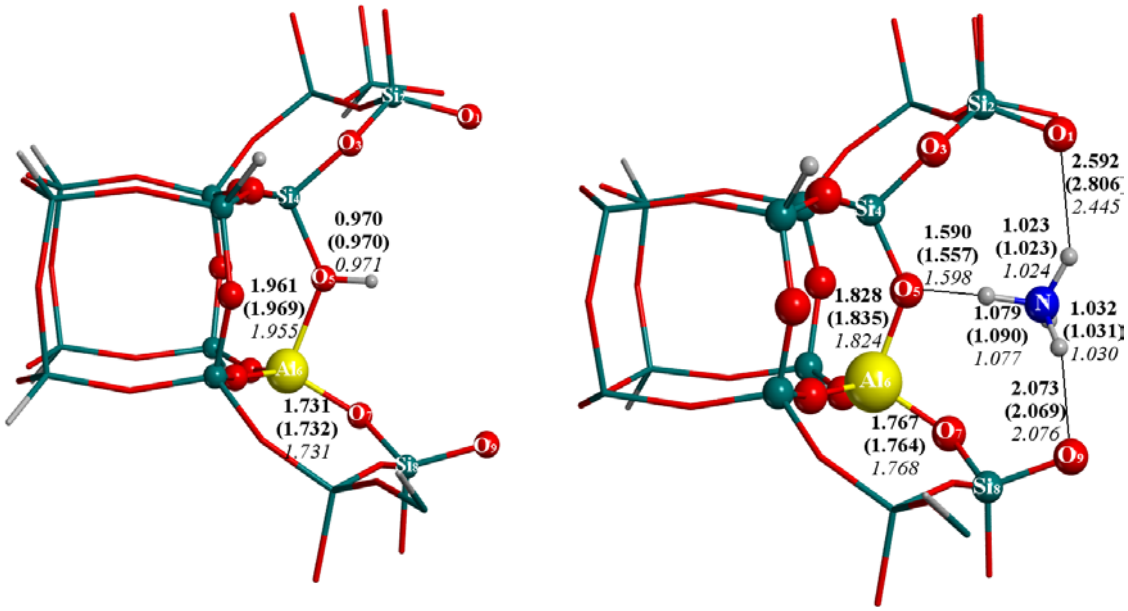

HZ **IP**

Figure 6.5 Optimised HZ and IP structures obtained with ONIOM approach and BSB. Bold values corresponds to B3LYP:MNDO level combination, in parenthesis B3LYP:AM1 ones and in Italic those obtained with B3LYP:HF. Distances are in Å

Table 6.4 Relative energies (kcal/mol) with respect to the HZ + NH_3 asymptote obtained with B3LYP/BSB as high level and the T12:T48 cluster[a]

Low-Level	ΔE	*HL*	*LL*
MNDO	–28.3(–26.3)	–27.8	–0.5
AM1	–25.1 (–23.1)	–27.3	+2.2
HF/3-21G	–31.0 (–28.8)	–28.0	–3.0
HF/3-21G//MNDO	–31.3 (–29.3)	–27.8	–3.5

[a] Relative energies corresponding to ONIOM2 calculations for cluster T12:T48 have been decomposed in two components:
$HL = E_C^{HL}(NH_4^+\text{-}Z^-) - E_C^{HL}(NH_3 + HZ)$
$LL = E_{real}^{LL}(NH_4^+\text{-}Z^-) - E_C^{LL}(NH_4^+\text{-}Z^-) - [E_{real}^{LL}(NH_3 + HZ) - E_C^{LL}(NH_3 + HZ)]$

To test the importance of including the channel in the inner part, we have performed single point calculations at the T12:T48 B3LYP/BSA:MNDO geometry increasing the size of the inner layer from T5 to T14. Figure 6.6 presents the considered clusters. Moreover, the electrostatic potential produced by the inner layer at the nitrogen position has been computed using the previous clusters. The used geometry is that of the adsorbed complex removing the ammonium ion. Table 6.5 presents the adsorption energies and the electrostatic potentials computed at the previous ONIOM clusters.

It is clearly observed that T5:T48 and T8:T48 underestimate considerably the adsorption energy, the obtained results being more similar to those obtained with free T5 than those obtained with periodic calculations. Two effects might be related to this fact. On one hand, two of the formed hydrogen bonds are not included in the inner layer. Moreover, as mentioned in the appendix, MNDO is not accurate enough to compute hydrogen bond interactions.

An important increase of the adsorption energy (–11.6 kcal/mol) is observed when one includes all the formed hydrogen bonds in the inner layer (cluster T10:T48). Moreover, little differences are observed between T10:T48 and T12:T48. A second jump in the adsorption energy (–6.2 kcal/mol) is observed when the cluster is terminated with Si-O-H instead of Si-H, indicating that these oxygen atoms still have an important role. However, it must be pointed out that T12+O:T48 and T14+O:T48 present higher absorption energies than that obtained with full periodic B3LYP calculation.

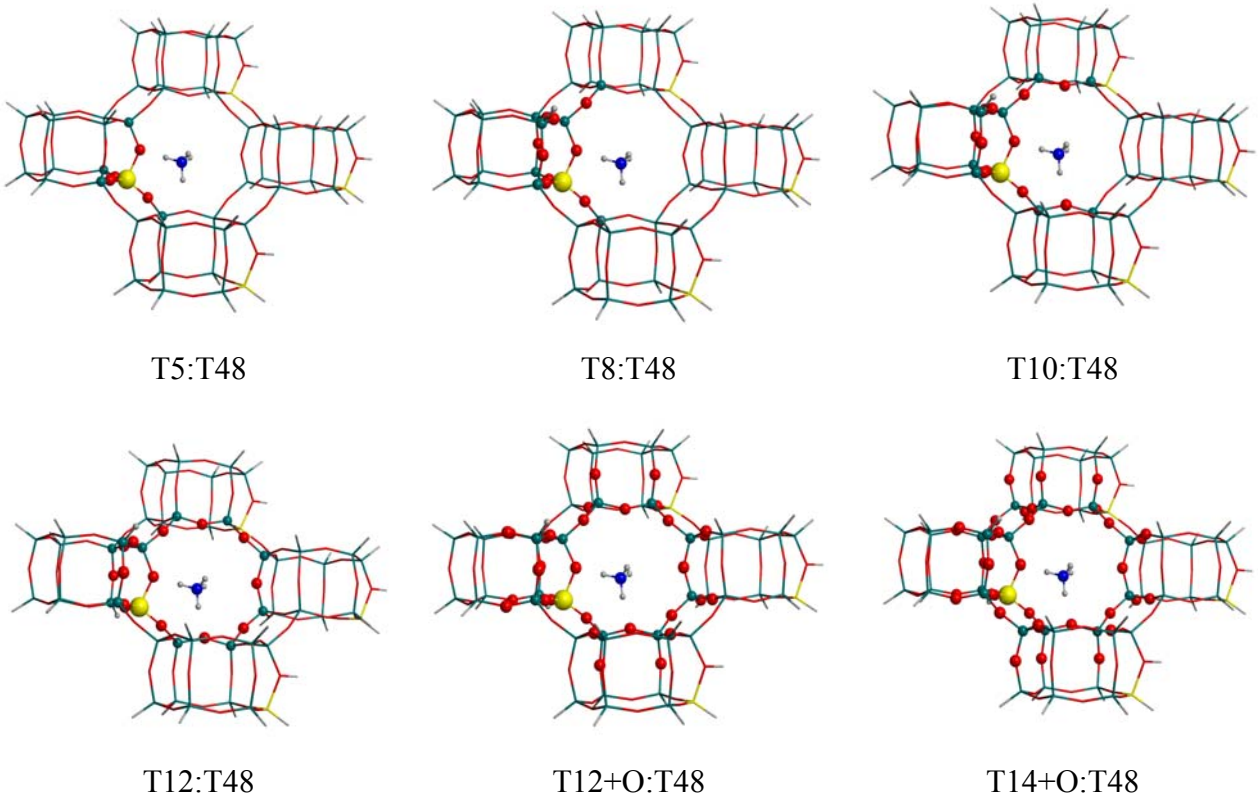

Figure 6.6 ONIOM2 clusters used to test the effect of enlarging the HL part. Solid atoms corresponds to those included in the high level cluster

Table 6.5. Adsorption energies (in kcal/mol) and electrostatic potential (in atomic units) using several ONIOM clusters at the B3LYP/BSA:MNDO level

Cluster	ΔE	Electrostatic Potential
T5:T48	–14.5	–0.129
T8:T48	–21.8	–0.127
T10:T48	–33.4	–0.129
T12:T48	–32.5	–0.134
T12+O:T48	–38.7	–0.162
T14+O:T48	–40.0	–0.159
Periodic	–36.9	

Brändle et al.[26] have also studied the adsorption of NH_3 on several zeolite frameworks using the embedded cluster approach. In agreement with the present results,

they also concluded that a T6 cluster, constructed to include all the oxygen atoms that may be involved in the formation of hydrogen bonds, is a big enough inner layer to reproduce the experimental adsorption energy. The only difference between our T10 cluster and the their T6 cluster is the inclusion of the four membered rings around the active site.

The electrostatic potential at the nitrogen position is negative and thus a positive charge would be stabilized. This negative value can be understood due to the fact that the global cluster has a negative charge and also due to the nonbonding pair electrons of the oxygen atoms of the channel that are pointing to the centre of the ring. This electrostatic potential could partially explain the fact that the ion pair structure is highly stabilized with respect to the HB structure. In addition to this, the electrostatic potential increases in absolute value when the size of the inner layer is increased. This result is in agreement with the variation of the adsorption energy.

The inclusion of the channel seems of great importance to give enough freedom to the system for the formation of more relaxed hydrogen bonds and to describe the electrostatic potential in the middle of the channel. Our results suggest that this potential is highly sensitive at least to all the ring structure and the following oxygens. Comparing the adsorption energies obtained with our biggest clusters and those obtained with periodic calculations the effects of further enlarging the cluster are expected to be small.

Taking as a reference the −36.9 kcal/mol periodic adsorption energy and considering the effect of BSSE (−4.9 kcal/mol) observed in ONIOM T12:T48 cluster, our best estimated value for the adsorption energy of NH_3 in acidic Chabazite is −32.0 kcal/mol which is very close to the experimental value obtained for zeolites with similar channel sizes.

6.5 Concluding remarks

The adsorption of NH_3 on HCHA has been studied using three different approaches: the T5 cluster, the ONIOM T12:T48 cluster and periodic calculations. Both periodic calculations and ONIOM results indicate that the adsorption of NH_3 on HCHA takes place through an ion pair structure produced by the deprotonation of the acidic Chabazite. These results are in agreement with the experimental evidences. The

ammonium ion is located in the eight-membered ring with three of its hydrogens forming hydrogen bonds with oxygens of the zeolite. In contrast, using the T5 cluster two minima are found; the NH_3-HZ hydrogen bonded structure and the NH_4^+-Z^- ion pair. These two structures are very similar in energy, in disagreement with experimental evidences.

Adsorption energies computed from B3LYP periodic calculations are in the range of the experimental values obtained for zeolites with similar channel sizes. However, the HF value is underestimated by about 25%.

All the considered ONIOM combinations lead to very similar structures around the active site. Thus, all considered low-levels impose similar constraints. However, larger differences are observed in the adsorption energies, mainly due to the different behaviour of the low-level contributions. It is observed that B3LYP:HF/3-21G combination is needed to reproduce the experimental adsorption energy. However, as all low-level introduce similar constraints the computationally expensive B3LYP:HF/3-21G optimisation can be avoided by performing only single point calculations at the B3LYP:MNDO optimised structure.

The analysis of the cluster size reveals that, the inclusion of the channel is of great importance to reproduce the adsorption energy of ammonia. However, the effect of the rest of the zeolite is found to be small. Therefore, cluster approaches may be enough to model related systems. Moreover, accurate enough results can be obtained with a T10:T48 cluster including all the oxygens of the zeolite involved in the hydrogen bonds.

References

(1) Smart, L.; Moore, E. Zeolites and related structures. In *Solid State Chemistry: An Introduction*; 2nd ed.; Chapman & Hall: London, 1995; pp 238.

(2) Farneth, W. E.; Gorte, R. J. *Chem. Rev.* **1995**, *95*, 615.

(3) Valyon, J.; Onyestyák, G.; Rees, L. V. C. *J. Phys. Chem. B* **1998**, *102*, 8994.

(4) Zecchina, A.; Geobaldo, F.; Spoto, G.; Bordiga, S.; Ricchiardi, G.; Buzzoni, R.; Petrini, G. *J. Phys. Chem.* **1996**, *100*, 16584.

(5) Yin, F.; Blumenfeld, A. L.; Gruver, V.; Fripiat, J. J. *J. Phys. Chem. B* **1997**, *101*, 1824.

(6) Pazé, C.; Bordiga, S.; Lamberti, C.; Salvalaggio, M.; Zecchina, A.; Bellussi, G. *J. Phys. Chem. B* **1997**, *101*, 4740.

(7) Paukshtis, E. A.; Malysheva, L. V.; Stepanov, V. G. *React. Kinet. Catal. Lett.* **1998**, *65*, 145.

(8) Barthos, R.; Lónyi, F.; Onyestyák, G.; Valyon, J. *J. Phys. Chem. B* **2000**, *104*, 7311.

(9) Lónyi, F.; Valyon, J. *Thermochimica Acta* **2001**, *373*, 53.

(10) Lónyi, F.; Valyon, J. *Micropor. and Mesopor. Mater.* **2001**, *47*, 293.

(11) Kao, H.-M.; Grey, C. P. *J. Phys. Chem.* **1996**, *100*, 5105.

(12) Kapustin, G. I.; Brueva, T. R. *Thermochimica Acta* **2001**, *379*, 71.

(13) Katada, N.; Igi, H.; Kim, J.-H.; Niwa, M. *J. Phys. Chem. B* **1997**, *101*, 5969.

(14) Brueva, T. R.; Mishin, I. V.; Kapustin, G. I. *Thermochimica Acta* **2001**, *379*, 15.

(15) Parrillo, D. J.; Gorte, R. J. *J. Phys. Chem.* **1993**, *97*, 8786.

(16) Lee, C.; Parrillo, D. J.; Gorte, R. J.; Farneth, W. E. *J. Am. Chem. Soc.* **1996**, *118*, 3262.

(17) Teunissen, E. H.; Jansen, A. P. J.; van Santen, R. A.; Orlando, R.; Dovesi, R. *J. Chem. Phys.* **1994**, *101*, 5865.

(18) Kassab, E.; Seiti, K.; Allavena, M. *J. Phys. Chem.* **1991**, *95*, 9425.

(19) Zygmunt, S. A.; Brand, H. V.; Lucas, D. J.; Iton, L. E.; Curtiss, L. A. *J. Mol. Struct.: Theochem* **1994**, *314*, 113.

(20) Teunissen, E. H.; van Santen, R. A.; Jansen, A. P. J.; van Duijneveldt, F. B. *J. Phys. Chem.* **1993**, *97*, 203.

(21) Kassab, E.; Fouquet, J.; Allavena, M.; Evleth, E. M. *J. Phys. Chem.* **1993**, *97*, 9034.

(22) Teunissen, E. H.; Jansen, A. P. J.; van Santen, R. A. *J. Phys. Chem.* **1995**, *99*, 1873.

(23) Kyrlidis, A.; Cook, S. J.; Chakraborty, A. K.; Bell, A. T.; Theodorou, D. N. *J. Phys. Chem.* **1995**, *99*, 1505.

(24) Vollmer, J. M.; Stefanovich, E. V.; Truong, T. N. *J. Phys. Chem. B* **1999**, *103*, 9415.

(25) Brändle, M.; Sauer, J.; Dovesi, R.; Harrison, N. M. *J. Chem. Phys.* **1998**, *109*, 10379.

(26) Brändle, M.; Sauer, J. *J. Am. Chem. Soc.* **1998**, *120*, 1556.

(27) Brändle, M.; Sauer, J. *J. Mol. Catal. A: Chemical* **1997**, *119*, 19.

(28) Yuan, S. P.; Wang, J. G.; Li, Y. W.; Jiao, H. *J. Phys. Chem. A* **2002**, *106*, 8167.

(29) Sierka, M.; Sauer, J. *J. Chem. Phys.* **2000**, *112*, 6983.

(30) Eichler, U.; Kölmel, C. M.; Sauer, J. *J. Comput. Chem. B* **1997**, *18*, 463.

(31) Vreven, T.; Morokuma, K. *J. Comput. Chem.* **2000**, *21*, 1419.

(32) Svensson, M.; Humbel, S.; Froese, R. D. J.; Matsubara, T.; Sieber, S.; Morokuma, K. *J. Phys. Chem.* **1996**, *100*, 19357.

(33) Maseras, F.; Morokuma, K. *J. Comput. Chem.* **1995**, *16*, 1170.

(34) Maseras, F.; Lledós, A.; Clot, E.; Eisenstein, O. *Chem. Rev.* **2000**, *100*, 601.

(35) Maseras, F.; Lledós, A. Computational Modeling for Homogeneous Catalysis. In *Computational Modeling of Homogeneous Catalysis*; Maseras, F., Lledós, A., Eds.; Kluwer Academic Publishers: Dordrecht, 2002; Vol. 25; pp 384.

(36) Roggero, I.; Civalleri, B.; Ugliengo, P. *Chem. Phys. Lett.* **2001**, *341*, 625.

(37) Erbetta, D.; Ricci, D.; Pacchioni, G. *J. Chem. Phys.* **2000**, *113*, 10744.

(38) Raksakoon, C.; Limtrakul, J. *J. Mol. Struct.: Theochem* **2003**, *631*, 147.

(39) Damin, A.; Bordiga, S.; Zecchina, A.; Lamberti, C. *J. Chem. Phys.* **2002**, *117*, 226.

(40) Damin, A.; Bordiga, S.; Zecchina, A.; Doll, K.; Lamberti, C. *J. Chem. Phys.* **2003**, *118*, 10183.

(41) Bonino, F.; Damin, A.; Bordiga, S.; Lamberti, C.; Zecchina, A. *Langmuir* **2003**, *19*, 2155.

(42) Lopez, N.; Pacchioni, G.; Maseras, F.; Illas, F. *Chem. Phys. Lett.* **1998**, *294*, 611.

(43) Hartree, D. R. *Proc. Cambridge Phil. Soc.* **1928**, *24*, 89.

(44) Fock, V. *Z. Physik* **1930**, *61*, 126.

(45) Becke, A. D. *J. Chem. Phys.* **1993**, *98*, 5648.

(46) Lee, C.; Yang, W.; Parr, R. G. *Phys. Rev. B* **1988**, *37*, 785.

(47) Pascale, F.; Ugliengo, P.; Civalleri, B.; Orlando, R.; D'Arco, P.; Dovesi, R. *J. Chem. Phys.* **2002**, *117*, 5337.

(48) Hehre, W. J.; Ditchfield, R.; Pople, J. A. *J. Chem. Phys.* **1972**, *56*, 2257.

(49) Dewar, M. J. S.; Thiel, W. *J. Am. Chem. Soc.* **1977**, *99*, 4899.

(50) Dewar, M. J. S.; Zoebisch, E. G.; Healy, E. F.; Stewart, J. J. P. *J. Am. Chem. Soc.* **1985**, *107*, 3902.

(51) Boys, S. F.; Bernardi, F. *Mol. Phys.* **1970**, *19*, 553.

(52) Saunders, V. R.; Dovesi, R. Roetti, C.; Orlando, R.; Zicovich-Wilson, C. M.; Harrison, N. M.; Doll, K.; Civalleri, B.; Bush, I. J.; D'arco, Ph.; Llunell, M. CRYSTAL03 development version

(53) Frisch, M. J.; Trucks, G. W.; Schlegel, H. B.; Scuseria, G. E.; Robb, M. A.; Cheeseman, J. R.; Zakrzewski, V. G.; Montgomery, J. A.; Stratmann, R. E.; Burant, J. C.; Dapprich, S.; Millam, J. M.; Daniels, A. D.; Kudin, K. N.; Strain, M. C.; Farkas, O.; Tomasi, J.; Barone, V.; Cossi, M.; Cammi, R.; Mennucci, B.; Pomelli, C.; Adamo, C.; Clifford, S.; Ochterski, J.; Petersson, G. A.; Ayala, P. Y.; Cui, Q.; Morokuma, K.; Malick, D. K.; Rabuck, A. D.; Raghavachari, K.; Foresman, J. B.; Cioslowski, J.; Ortiz, J. V.; Baboul, A. G.; Stefanov, B. B.; Liu, G.; Liashenko, A.; Piskorz, P.; Komaromi, I.; Gomperts, R.; Martin, R. L.; Fox, D. J.; Keith, T.; Al-Laham, M. A.; Peng, C. Y.; Nanayakkara, A.; Gonzalez, C.; Challacombe, M.; Gill, P. M. W.; Johnson, B. G.; Chen, W.; Wong, M. W.; Andres, J. L.; Head-Gordon, M.; Replogle, E. S.; Pople, J. A. Gaussian 98; Gaussian Inc.: Pittsburgh, 1998.

(54) Eichler, U.; Brändle, M.; Sauer, J. *J. Phys. Chem. B* **1997**, *101*, 10035.

(55) Sierka, M.; Eichler, U.; Datka, J.; Sauer, J. *J. Phys. Chem. B* **1998**, *102*, 6397.

(56) Chatterjee, A.; Iwasaki, T.; Ebina, T.; Miyamoto, A. *Micropor. and Mesopor. Mater.* **1998**, *21*, 421.

7. Summary and conclusions

In the present thesis four different processes related with Cu^+ and H^+ exchanged zeolites have been studied. Each process has been presented in a separated chapter and the specific conclusions have been included in the corresponding concluding remarks of each chapter. Therefore, in the present section we will summarize the main results of each chapter. Moreover, we will present general conclusions about the modelling of zeolites obtained from the experience achieved during the thesis

A. Cu^+ exchanged zeolites

Chapter 3 presents the study of the decomposition of the environmental undesired NO by CuZSM-5. In particular, we have analysed the viability of the postulated mechanism C (see page 37). For this purpose many possible intermediate structures have been explored. Several ligand conformations as well as spin multiplicities have been considered. Present results show that $(NO_2)(NO)CuZ$ or $(N_2O_3)CuZ$ species are not relevant intermediates in the NO decomposition process since, although they are very stable, their decomposition energy barriers are very high. However, at high temperatures the interaction of two NO molecules with (O)CuZ might evolve to products through a [(ONNOO)CuZ] transition state structure.

In chapter 4, the H_2 adsorption at different coordination sites of Cu^+ cations in Chabazite is reported. Periodic calculations have been performed to analyse the different possible locations of Cu^+ cations. The effect of the zeolite framework in the Cu^+-H_2 interaction is analysed by comparison between periodic and cluster calculations. The obtained results explain the experimental observations and confirm that Cu^+ zeolites may be more suitable sieves for H_2 storage than alkali metal exchanged zeolites.

At this point, it can be concluded that Cu^+ cations coordinated to only two oxygen atoms of the zeolite framework are the most active Cu^+ sites for the adsorption of ligands. After the adsorption of one or two ligands, these cations are usually in a square-planar environment. Moreover, in Cu^+ exchanged zeolites, the zeolite framework favours the charge transfer from the metal cation to the ligand. This increase of charge transfer is due to the polarisation of copper 3d orbitals produced by the non-bonding oxygen p orbitals of the zeolite where Cu^+ is coordinated. This charge transfer is maximal when the ligand lies in the CuZ plane.

B. H^+ exchanged zeolites

H^+ exchanged zeolites have been used to test the reliability of the hybrid ONIOM approach to model zeolites, since the absence of transition metals allows the use of semiempirical methods. Periodic calculations have been shown to be an essential tool to establish target values to be compared with.

Chapter 5 describes the keto-enol isomerization of acetaldehyde in HZSM-5 that is the rate determinant step in the aldol condensation. The catalytic activity of the zeolite is compared to the process catalysed by a water molecule and an important decrease of the energy barrier is observed. Moreover, both reactant and product are found to be hydrogen bonded complexes. Results obtained with clusters of different sizes and using the hybrid ONIOM methodology have been discussed.

In chapter 6, the NH_3 adsorption on acidic Chabazite has been studied. We have chosen ammonia as probe molecule since the nature of the interaction is known and experimental data is available. Moreover, given that long range effects have been suggested to be very important, the NH_3 adsorption on Chabazite is a critical test for ONIOM approach. Results have pointed out the importance of cluster size for studing this system, the nature of the interaction (through an ion pair structure) and adsorption energy being only well described with periodic calculations or with ONIOM calculations that include the eight membered ring in the inner part.

The present H^+ exchanged zeolite studies allow us to conclude that the effect of increasing the zeolite framework is more important for species that interact through an ion pair structure than for hydrogen bonded ones.

C. Zeolite modelling

The comparison with periodic calculations as well as previous QM-Pot studies reveals that accurate enough results for metal exchanged zeolites can be obtained using small clusters such as T3, which include the nearest environment of the metal cation. In contrast, for H^+ exchanged zeolites, the results obtained show that small clusters are not suitable models.

Two factors seem determinant. On one hand the substitution of Cu^+ per H^+ leads to less constrained clusters which easily evolve to structures with unrealistic interactions. On the other hand, the role of the zeolite framework can be more important in proton exchanged zeolites. In particular, present results show that clusters must include the channel where the chemical process takes place if one wants to obtain results similar to those from periodic calculations.

ONIOM scheme seems to be a good strategy to introduce geometry constraints of the zeolite framework. However, reliable energies are only obtained if the inner layer includes at least all the oxygen atoms of the zeolite that are involved in the hydrogen bonds.

In the last years important developments in the modelling of solids and extended systems such as zeolites have been achieved. In particular, recent implementations of density functional methods in several periodic packages that allow geometry optimisations is remarkable. However, the computational cost of periodic calculations is still very high for many systems. Several less computationally demanding approaches can be found in the literature and some of them have been used in the present thesis bringing to highly satisfactory results. However, there are no general rules that indicate the way how they must be used and thus, they should be calibrated for each system by comparison with periodic calculations (when feasible) and with available experimental data.

Appendix:
Computational methods

A.1 Quantum chemical methods

The aim of most of quantum chemical methods is to solve the time independent Schrödinger equation.

$$\hat{H}\Psi(r,R) = E\Psi(r,R) \qquad (A.1)$$

where $\hat{H}$ is the Hamiltonian operator for the system, Ψ is the wave function of the system which depends on the electron (r) and nuclei (R) coordinates and E is its energy.

Since electrons are much lighter than nuclei, electrons would move faster, and thus one can assume that they would be instantaneously adapted to any new nuclei configuration. This is known as the Born-Oppenheimer approximation. In this approximation one must solve first the electronic Schrödinger equation:

$$\hat{H}_{el}\Psi_{el}(r;R) = E_{el}(R)\Psi_{el}(r;R) \qquad (A.2)$$

where $\hat{H}_{el}$ is the electronic Hamiltonian, Ψ_{el} is the electronic wave function of the system which depends on the electron coordinates (r) and parametrically on the nuclei coordinates (R) and E_{el} is the electronic energy.

A.1.1 Hartree-Fock approximation

The electronic Schrödinger equation is only resoluble for molecules with one electron, so further approximations must be done for larger systems. The Hartree-Fock method[1,2] applies the variational principle using as a trial function a Slater determinant, which are antisymmetrized products of monoelectronic functions or spin-orbitals.

Spin-orbitals (χ) are the product of two parts, molecular orbital and the spin function. Molecular orbitals (ψ) are built by a linear combination of atomic basis functions (LCAO) which reduces the problem of the minimization of the energy to find the appropriate coefficients for this linear combination. These coefficients are found solving the Roothan equations.

This approximation assumes that each electron is moving in an average field created by nuclei and the other electrons and the instantaneous repulsion between electrons is not considered. So that, the movement of electrons is not correlated.

The number and type of basis functions strongly influence the quality of the results. The use of a single basis function for each atomic orbital leads to the minimal basis set. In order to improve the results, extended basis should be used. These basis sets are named double-ζ, triple-ζ, etc. depending on whether each atomic orbital is described by two, three, etc. basis functions. Higher angular momentum functions, called polarization functions, are also necessary to describe the distortion of the electronic distribution due to the bonding. Finally, diffuse functions with smaller exponents but the same angular momentum allow the electron density to be more expanded.

The cost of performing a HF calculation scales formally as the fourth power of the number of basis functions.[3-5] This arises from the number of two-electron integrals. Semiempirical methods reduce the computational cost by reducing the number of these integrals that are computed. That is they are neglected or made into parameter. Moreover, semiempirical methods only consider the valence orbitals that are represented with a minimal basis set, while internal electrons and nucleus of each atom are considered as a core. Within semiempirical methods there are several different approaches to reduce the computation of two-electron integrals. MNDO[6] (modified Neglect of Diatomic integrals) and AM1[7] (Austin Model 1), the semiempirical methods used in this thesis, are parameterisations of NDDO[8] (Neglect of Diatomic Differential Overlap) approximation where the bielectronic integrals are parameterised except those representing the diatomic overlap that are neglected. AM1 was created to correct some bad descriptions of MNDO,[4] one of these improvements was in the description of hydrogen bonds.

A.1.2 Methods for introducing the electron correlation.

Increasing the basis set dimension leads to better results. However, with a monoconfigurational function one will never obtain the exact result and that is due to the absence of electron correlation. The best Hartree-Fock energy would be obtained with an infinite basis set and this is called the Hartree-Fock limit. The correlation energy is defined as the difference between the exact energy and the Hartree-Fock limit.

Two types of electronic correlation can be distinguished. The dynamic correlation is due to the fact that Hartree-Fock approximation does not consider the instantaneous repulsion between electrons. The non-dynamic correlation appears when different electronic configurations are close in energy and they are strongly mixed in the wave function.

Several approaches have been developed to treat electron correlation. Most of these methods start from a single-reference Hartree-Hock wave function. In the configuration interaction (CI) method,[9-11] the wave function is expanded over a large number of configurations obtained by exciting electrons from occupied to unoccupied orbitals. The coefficients of such an expansion are determined variationally. Given that the consideration of all possible excitations (Full CI) is not computationally feasible for most of the molecules, the expansion is truncated. The most common approach is CISD, where only single and double excitations are considered. The Møller-Plesset (MP) perturbation theory[12] is based on a perturbation expansion of the energy of the system. The *n*th-order treatment is denoted MP*n* . MP2 is the computationally cheapest treatment and MP4 is the highest order normally used. Finally, other methods for including dynamical electron correlation are those based on the coupled cluster approach[13] which is based on a different definition of the wave function. The most common Coupled Cluster methods are CCSD (coupled Cluster singles and doubles) and CCSD(T)[14] where triple excitations are also included perturbatively.

When the HF wave function gives a very poor description of the system, i.e. when nondynamical electron correlation is important, the multiconfigurational (MCSCF) method is used. This method is based on a CI expansion of the wave function in which both the coefficients of the CI and those of the molecular orbitals are variationally determined. One of the most popular approaches is the Complete Active Space Self-consistent Field method (CASSCF).[15] The selection of configurations is done by partitioning the MOs into active and inactive spaces. The active MOs correspond to the highest occupied orbitals and lowest unoccupied ones from a HF calculation. The inactive MOs either have 2 or 0 electrons, that is, they are always empty or doubly occupied. Within the active molecular orbitals a Full CI is performed. The choice of active and inactive Molecular Orbitals is done manually, by considering the chemical problem and the computational cost. It must be pointed out that in all the points

considered in a potential energy surface the active space should be the same and include all the orbitals which change significantly between them. A common notation of CASSCF is CASSCF(n,m) where n is the number of electrons and m is the number of orbitals.

A.1.3 Density functional theory

An alternative approach to conventional methods is the density functional theory (DFT). This theory is based on the use of the electron density to obtain the energy of the ground state.

Electron density is defined as the following multiple integral over the spin coordinates of electrons and over all but one of the spatial variables $(\vec{r})$ [16,17]

$$\rho(\vec{r}_1) = N\int\ldots\int|\Psi(\vec{x}_1,\vec{x}_2,\ldots,\vec{x}_N)|^2 ds_1 d\vec{x}_2\ldots d\vec{x}_N \qquad (A.3)$$

$\rho(r)$ determines the probability of finding any of the N electrons within the volume $d\vec{r}_1$ but with arbitrary spin while the other N-1 electrons have arbitrary positions and spins. $\rho(r)$ is non-negative function of only the three spatial variables that vanishes at infinity and integrates to the total number of electrons.

$$\rho(r\to\infty) = 0 \qquad (A.4)$$

$$\int\rho(r)d\vec{r}_1 = N \qquad (A.5)$$

Unlike the wave function, the electron density is an observable and can be measured experimentally.

A.1.3.1 The Hohenberg-Kohn Theorems

Density functional theory as we know it today was born in 1964 when Hohenberg and Kohn stated and proved two base theorems.[18] Considering a system of N electrons described by the non-relativistic Hamiltonian, the first Hohenberg-Kohn Theorem states that any observable of a ground stationary non-degenerate state of a N-particle system could be determined from the electron density ρ of this ground state. Thus, these

observables could be written as a functional of the electron density of the ground state. In particular the electronic energy functional could be written as:

$$E[\rho] = T[\rho] + W_{XC}[\rho] + E_{ext}[\rho] \qquad (A.6)$$

where $T[\rho]$ is the kinetic energy, $W_{xc}[\rho]$ is the exchange-correlation energy and $E_{ext}[\rho]$ is the external potential (normally the repulsion between electrons and nuclei).

Up to this point it is established that the ground state density is sufficient to obtain all properties of interest. However, one does not still have any tool to obtain the ground state density. The second Hohenberg-Kohn theorem states that the energy obtained with the functional (A.6) and any trial density $[\tilde{\rho}]$, which satisfies the necessary boundary conditions, represents an upper limit to the true ground state energy E_0.

$$E_0 \leq E[\tilde{\rho}] = T[\tilde{\rho}] + W_{XC}[\tilde{\rho}] + E_{ext}[\tilde{\rho}] \qquad (A.7)$$

These two theorems tell us that a unique mapping between the ground state density $\rho(r)$ and the ground state energy E_0 exists in principle. However, they do not provide any guidance at all how the functional should be constructed. In particular from equation A.6 the kinetic energy, $T[\rho]$, and the exchange-correlation term, $W_{XC}[\rho]$, functionals are unknown, so that an approximation of them should be made.

A.1.3.2 The Kohn-Sham approach

Kohn and Sham in 1965 suggested how the energy functional could be approached.[19] They tried to find an accurate way to treat the kinetic energy in DFT theory. The kinetic energy is easily calculated if Ψ is known. So that, Kohn and Sham proposed an indirect procedure to obtain an approximation of $T[\rho]$ using a self-consistent method involving monoelectronic wave functions. They introduce a non-interacting N-electrons system with an external potential $V_s(r)$. This potential $V_s(r)$ is presumed to be such that the ground-state density of this non-interacting system is equal to the exact density of the real system. That is, the reference system presents the same electron density as the real system. For this reference system, the electronic Hamiltonian only presents monoelectronic terms.

$$\hat{H}_S = -\frac{1}{2}\sum_i^N \nabla_i^2 + \sum_i^N V_S(\vec{r}_i) \qquad (A.8)$$

And the exact wave function is a Slater Determinant

Thus the electron density could be reproduced solving the N-monoelectronic equation

$$\hat{h}^{KS}\chi_i = \varepsilon_i \chi_i \qquad (A.9)$$

These equations are called the Kohn-Sham equations, where $\hat{h}^{KS}$ is called the Kohn-Sham operator and χ_i are called the Kohn-Sham spin-orbitals. Thus, the exact kinetic energy could be computed as

$$T_s = \frac{1}{2}\sum_i^N \langle \chi_i | \nabla^2 | \chi_i \rangle \qquad (A.10)$$

Here the subindex s indicates that this kinetic energy is the one for the non-interacting reference system which is non-equal to the real kinetic energy. This makes us to redefine the energy functional as

$$E[\rho] = T_S[\rho] + E_{XC} + E_{ext} \qquad (A.11)$$

where now E_{XC} could be expressed as:

$$E_{XC} = (T[\rho] - T_s[\rho]) + W_{XC} \qquad (A.12)$$

And this means that it is formed by the residual kinetic energy and the non-classical electron interactions, that is, it contains everything that is unknown.

The Kohn-Sham equations must be solved iteratively until the self-consistency is achieved.

Up to this point the method will bring to the exact solution if the E_{XC} were known. However as mentioned before this is not possible, so that some approximations must be done.

A.1.3.3 LDA, GGA and Hybrid functionals

In the majority of DFT approximations the E_{XC} functional is divided in two parts:

$$E_{XC}[\rho] = E_X[\rho] + E_C[\rho] \qquad (A.13)$$

where E_X is defined as the exchange energy and physically introduces the non-Coulombic interaction between electrons with same spin density and E_C is the correlation energy, includes the interaction between electrons with different spin densities. Normally the exchange contributions are significantly larger in absolute numbers.

In LDA, it is assumed that the E_{XC} functional only depends on the electron density, treated as a uniform gas of electrons. The exchange part is given by the Dirac formula,[20] while the correlation term has been obtained by Vosko, Wilk and Nusair from Montecarlo simulations.[21] Several acronyms, such as LDA, LSDA and SVWN, might be found in the literature referring to LDA approximation functional.

New functionals to improve the LDA results appeared in the eighties when expansions to the LDA functionals were developed. The logical first step in that direction was the use not only of the density in each point $\rho(r)$ but also the information about the gradient of the density $\nabla\rho(r)$ in that point, in order to account for the non-homogeneity of true electron density. These methods are termed generalized gradient approximation (GGA). As mentioned above, E_{XC}^{GGA} is usually divided in two terms E_X and E_C and approximations for the two terms are formulated individually.

Several functionals appeared depending on the modelling of this gradient contribution. For the exchange term, nowadays the Becke functional (B)[22] is the one most widely used. On the other hand, the most common GGA correlation functionals are the Perdew 86 (P86),[23] the Perdew-Wang 1991 (PW91)[24,25] and the Lee, Yang and Parr (LYP)[26] functionals. Thus, the combination of Becke exchange functional with P86, PW91 and LYP correlation ones leads to the BP86, BPW91 and BLYP functionals, respectively.

To improve the results of GGA functionals, hybrid functionals introduce in the exchange functional the Hartree-Fock exchange energy. This contribution is not local, so that hybrid functionals are non-local functionals. The main problem is to determine the

appropriate contribution of the Hartree-Fock term which is generally done by fitting the parameters to experimental data.

The first hybrid functional developed was the Half and Half hybrid functional which includes 50% of the HF exchange energy.[27] That is:

$$E_{XC}^{BH} = 0.5E_{X}^{HF} + 0.5E_{XC}^{LDA} \qquad (A.14)$$

However, it was observed that the HF energy contribution was too high, so that Becke developed the well-known Becke 3 functional fitting three parameters which fix the LDA, HF and gradient correction contributions.[28] These parameters were fitted from experimental data of ionising potentials, electron affinities and atomic energies. The resulting functional is expressed as:

$$E_{XC}^{B3} = (1 - a)\, E_{X}^{LDA} + aE_{X}^{HF} + b\Delta E_{X}^{B} + E_{C}^{LDA} + c\Delta E_{C}^{GGA} \qquad (A.15)$$

where a= 0.2, b= 0.72 and c = 0.81

These hybrid functionals can be combined with different GGA correlation functionals obtaining the so-called BHLYP (when Half and Half functional is combined with Lee Yang and Parr one), B3PW91 (Becke 3 and Perdew Wang 1991) or B3LYP (Becke 3 and Lee Yang and Parr). B3LYP is probably the hybrid functional most largely used and it is the functional that has been mainly used in the present thesis.

A.2 Potential energy surface

One of the main consequences of the Born-Oppenhimer approximation is that the nuclei move on a potential energy surface obtained by solving the electronic problem and adding the nuclear-nuclear repulsion. These surfaces are continuous and continuously differentiable. Moreover, as the potential energy surface arises from the solution of the electronic problem, there is a different surface for each electronic state. These surfaces for non-linear molecules depend on 3N-6 variables (where N is the number of nuclei) and describe the movement of the nuclei. However, normally the information needed can be obtained from the analysis of some specific points, the stationary points.

Stationary points are those points in the potential energy surface which present a gradient equal to 0. Two different kinds of stationary points are defined regarding the second derivative matrix or Hessian matrix. If all eigenvalues of the Hessian matrix are positive values any small displacement around that stationary point will have higher energy so that these points are minimum of the potential energy surface and correspond to equilibrium geometries of the studied system. On the other hand, if at least one of the eigenvalues is negative, the stationary point present at least one direction which presents a decay in energy. This points are known as saddle points. Special interest presents those saddle points with only one negative eigenvalue which are associated to transition state structures, that is the highest energy point of the lowest energy path connecting reactants and products.

Thus by comparison of different minima in the potential energy surface one obtains the relative energetics of equilibrium geometries (for example reactants and products) and by comparison of transition state structures one could have an idea of the reaction easiness and which mechanism is favoured.

A.6. Potential energy surface intersections

As mentioned above each electronic state describes one potential energy surface. These surfaces can present different relative stabilities depending on the nuclear coordinates indicating an electronic state change.

The intersection between two potential energy surfaces of the same spin multiplicity takes place in a conical intersection.[29,30] Conical intersections are characterised by two directions x_1 and x_2.[30,31]

$$x_1 = \frac{\partial(E_a - E_b)}{\partial Q} \qquad (A.16) \qquad x_2 = \left\langle \Psi_a \left| \frac{\partial \hat{H}}{\partial Q} \right| \Psi_b \right\rangle \qquad (A.17)$$

x_1 corresponds to the gradient difference between both states, and x_2 is the gradient of the coupling vector between both states, E_a and E_b are the energies of state a and b respectively and Ψ_a and Ψ_b are their functions obtained from a CI calculation. Plotting the energy in the subspace of these two geometric variables the potential energy would have the form o a double cone in the region of degeneracy.

Any movement on the plane defined by x_1 and x_2 lifts the degeneracy, so that the intersection of the two states is formed by infinite points. Thus the energy is not minimized in N-1 dimensions as in the transition states. It is minimized in the remaining N-2 variables (excluding x_1 and x_2). For an intersection between two different spin multiplicity states, the dimension of crossing surface is N-1.

In reactions involving different states for reactants and products the conical intersection has a similar role as the transition state for conventional reactions, that is the highest energetic structure connecting the lowest energetic path.[30]

We are interested in the lowest energy point of this surface that corresponds to a well-defined geometry of the system.[32,33] One must do a constrained optimisation with an ab-initio method which describes the excited states properly. Normally MRSCF methods are used and especially CASSCF. The lowest energy point on a conical intersection is obtained by minimising the energy in intersection space.

In particular, the method used in the present thesis to localise conical intersections is that developed by Robb and co-workers[33] which is implemented in GAUSSIAN-98.[34] Thus, we have used CASSCF level with state-averaged orbitals with a weighting of 50%/50% to the singlet and triplet states.

References

(1) Hartree, D. R. *Proc. Cambridge Phil. Soc.* **1928**, *24*, 89.

(2) Fock, V. *Z. Physik* **1930**, *61*, 126.

(3) Bertran, J.; Branchadell, V.; Moreno, M.; Sodupe, M. *Química Cuántica*; Síntesis: Madrid, 2000.

(4) Jensen, F. *Introduction to Computational Chemistry*; John Wiley and Sons: Chichester, 2002.

(5) Stewart, J. J. P. Semiempirical Methods: Integrals and Scaling. In *Encyclopedia of Computational Chemistry*; von Ragué-Schleyer, P., Ed.; John Wiley and Sons: Chichester, 1998; Vol. 4; pp 2574.

(6) Dewar, M. J. S.; Thiel, W. *J. Am. Chem. Soc.* **1977**, *99*, 4899.

(7) Dewar, M. J. S.; Zoebisch, E. G.; Healy, E. F.; Stewart, J. J. P. *J. Am. Chem. Soc.* **1985**, *107*, 3902.

(8) Pople, J. A.; Beveridge, D. L. *Approximate Molecular Orbital Theory*; McGraw-Hill: New York, 1970.

(9) Shavitt, I. *Methods of Electronic Structure Theory*; Schaefer III, Plenum: New York, 1977.

(10) Roos, B. *Chem. Phys. Lett.* **1972**, *15*, 153.

(11) Knowles, P. J.; Handy, N. C. *Chem. Phys. Lett.* **1984**, *111*, 315.

(12) Møller, C.; Plesset, M. S. *Phys. Rev.* **1934**, *46*, 618.

(13) Čížek, J. *J. Chem. Phys.* **1966**, *45*, 4256.

(14) Raghavachari, K.; Trucks, G. W.; Pople, J. A.; Head-Gordon, M. *Chem. Phys. Lett.* **1989**, *157*, 479.

(15) Roos, B. O. *Adv. Chem. Phys.* **1987**, *69*, 399.

(16) Koch, W.; Holthausen, M. C. *A Chemist's Guide to Density Functional Theory*, second ed.; John Wiley and Sons: Weinheim, 2001.

(17) Caballol, R.; Solà, M. Métodos de la Química Cuántica. In *Química Teórica y Computacional*; Andrés, J., Bertran, J., Eds.; Publicacions de la Universitat Jaume I: Castelló de la Plana, 2000; pp 80.

(18) Hohenberg, P.; Kohn, W. *Phys. Rev.* **1964**, *136*, B864.

(19) Kohn, W.; Sham, L. J. *Phys. Rev.* **1965**, *140*, A1133.

(20) Slater, J. C. *Quantum Theory of Molecules and Solids*; McGraw-Hill: New York, 1974; Vol. 4.

(21) Vosko, S. H.; Wilk, L.; Nusair, M. *Can. J. Phys.* **1980**, *58*, 1200.

(22) Becke, A. D. *Phys. Rev. A* **1988**, *38*, 3098.

(23) Perdew, J. P. *Phys. Rev. B* **1986**, *33*, 8822.

(24) Perdew, J. P.; Chevary, J. A.; Vosko, S. H.; Jackson, K. A.; Pederson, M. R.; Singh, D. J.; Fiolhais, C. *Phys. Rev. B* **1992**, *46*, 6671.

(25) Perdew, J. P.; Wang, Y. *Phys. Rev. B* **1992**, *45*, 13244.

(26) Lee, C.; Yang, W.; Parr, R. G. *Phys. Rev. B* **1988**, *37*, 785.

(27) Becke, A. D. *J. Chem. Phys.* **1993**, *98*, 1372.

(28) Becke, A. D. *J. Chem. Phys.* **1993**, *98*, 5648.

(29) Teller, E. *J. Phys. Chem.* **1937**, *41*, 109.

(30) Bernardi, F.; Olivucci, M.; Robb, M. A. *Chem. Soc. Rev.* **1996**, 321.

(31) Robb, M. A.; Olivucci, M.; Bernardi, F. Photochemistry. In *Encyclopedia of Computational Chemistry*; von Ragué-Schleyer, P., Ed.; John Wiley and Sons: Chichester, 1998; Vol. 3; pp 2056.

(32) Bearpark, M. J.; Robb, M. A.; Schlegel, H. B. *Chem. Phys. Lett.* **1994**, *223*, 269.

(33) Ragazos, I. N.; Robb, M. A.; Bernardi, F.; Olivucci, M. *Chem. Phys. Lett.* **1992**, *197*, 217.

(34) Frisch, M. J.; Trucks, G. W.; Schlegel, H. B.; Scuseria, G. E.; Robb, M. A.; Cheeseman, J. R.; Zakrzewski, V. G.; Montgomery, J. A.; Stratmann, R. E.; Burant, J. C.; Dapprich, S.; Millam, J. M.; Daniels, A. D.; Kudin, K. N.; Strain, M. C.; Farkas, O.; Tomasi, J.; Barone, V.; Cossi, M.; Cammi, R.; Mennucci, B.; Pomelli, C.; Adamo, C.; Clifford, S.; Ochterski, J.; Petersson, G. A.; Ayala, P. Y.; Cui, Q.; Morokuma, K.; Malick, D. K.; Rabuck, A. D.; Raghavachari, K.; Foresman, J. B.; Cioslowski, J.; Ortiz, J. V.; Baboul, A. G.; Stefanov, B. B.; Liu, G.; Liashenko, A.; Piskorz, P.; Komaromi, I.; Gomperts, R.; Martin, R. L.; Fox, D. J.; Keith, T.; Al-Laham, M. A.; Peng, C. Y.; Nanayakkara, A.; Gonzalez, C.; Challacombe, M.; Gill, P. M. W.; Johnson, B. G.; Chen, W.; Wong, M. W.; Andres, J. L.; Head-Gordon, M.; Replogle, E. S.; Pople, J. A. Gaussian 98; Gaussian Inc.: Pittsburgh, 1998.